Enstrophy and passive scalar transport near the turbulent/non-turbulent interface in a turbulent planar jet flow

Cite as: Phys. Fluids **26**, 105103 (2014); https://doi.org/10.1063/1.4898208
Submitted: 13 March 2014 • Accepted: 02 October 2014 • Published Online: 22 October 2014

T. Watanabe, Y. Sakai, K. Nagata, et al.

PHYSICS OF FLUIDS **26**, 105103 (2014)

Enstrophy and passive scalar transport near the turbulent/non-turbulent interface in a turbulent planar jet flow

T. Watanabe,[1,a)] Y. Sakai,[1] K. Nagata,[1] Y. Ito,[1] and T. Hayase[2]
[1]*Department of Mechanical Science and Engineering, Nagoya University, Nagoya, Japan*
[2]*Institute of Fluid Science, Tohoku University, Sendai, Japan*

(Received 13 March 2014; accepted 2 October 2014; published online 22 October 2014)

The enstrophy ($\omega^2/2$) and passive scalar (ϕ) transport near the turbulent/non-turbulent (T/NT) interface is investigated using direct numerical simulation of a planar jet with passive scalar transport. To take into account the interface movement, we derive the transport equations for the enstrophy and the scalar in a local coordinate system moving with the T/NT interface. The characteristics of the T/NT interface are analyzed for three interface orientations. The cross-streamwise edge and the leading edge face the cross-streamwise and streamwise directions, respectively, and the trailing edge is opposite to the leading edge. The propagation velocity of the T/NT interface is derived from the enstrophy transport equation in the local coordinate system. The T/NT interface propagates toward the non-turbulent region on average at the cross-streamwise and leading edges, whereas the trailing edge frequently propagates into the turbulent region. The conditional average of the enstrophy transport equation in the local coordinate system shows that viscous diffusion transports, toward the non-turbulent region, enstrophy, that is advected from the turbulent core region or is produced slightly inside the T/NT interface. Viscous diffusion contributes greatly to the enstrophy growth in the region very close to the T/NT interface. The transport equation for the scalar ϕ in the local coordinate system is used to analyze the scalar transport near the T/NT interface. The conditional average of the advection term shows that ϕ in the non-turbulent region is frequently transported into the turbulent region across the cross-streamwise and leading edges by interface propagation toward the non-turbulent region. In contrast, ϕ in the turbulent region is frequently transported into the non-turbulent region across the trailing edge. The conditional averages of the advection and molecular diffusion terms show that both the interface propagation and the molecular diffusion contribute to the scalar transport across the T/NT interface. [http://dx.doi.org/10.1063/1.4898208]

I. INTRODUCTION

Free shear flows, such as wakes, jets, and mixing layers, can be distinguished into two regions: a turbulent region characterized by high vorticity, and a non-turbulent region consisting of irrotational flows. These two regions are divided by a sharp interface, which is referred to as the turbulent/non-turbulent (T/NT) interface.[1] The T/NT interface plays an important role in the development of free shear flows. A non-premixed jet flame is a typical example in which the T/NT interface is important. In the non-premixed jet flame, the fuel and oxidizer are mixed and chemical reactions occur near the interface between the jet and the ambient flows.[2,3] Thus, it is desirable to investigate the characteristics of the T/NT interface in order to develop engineering equipment (e.g., mixers, chemical reactors, and combustors).

[a)]Research Fellow of the Japan Society for the Promotion of Science. watanabe.tomoaki@c.nagoya-u.jp

The T/NT interface has been investigated recently by experimental, numerical, and analytical approaches. In the numerical approach, direct numerical simulation (DNS) is useful for investigating the T/NT interface because it provides all the components of the vorticity vector, which is used to detect the interface. On the other hand, a passive scalar is often used as a marker of the turbulent region instead of the vorticity vector in experiments[4–6] and large eddy simulations.[7] Bisset *et al.* used the DNS results for wakes behind a flat plate to investigate the characteristics of the flow and scalar fields near the T/NT interface.[8] They introduced conditional statistics conditioned on the distance from the T/NT interface. Conditional statistics have been widely used in studies of the T/NT interface. da Silva and Pereira[9] investigated the invariants of the velocity gradient, rate of strain, and rate of rotation tensors near the T/NT interface by using DNSs of a temporally developing jet,[10] and showed that some distance is required for the adjustment of statistical properties of the invariants between the T/NT interface and the turbulent region. DNSs of a temporally developing jet were also used to investigate the thickness of the T/NT interface,[11] the vorticity structure near the T/NT interface,[12] and the kinetic energy budget near the T/NT interface.[13] These studies showed that the thickness of the T/NT interface is of the order of the Taylor microscale, which is almost equal to the radius of large vorticity structures near the interface.

Mathew and Basu[14] showed that the entrainment process occurs at small scales using temporal DNS of a circular shear layer. Westerweel *et al.* used particle image velocimetry and laser-induced fluorescence to experimentally investigate the T/NT interface in a round jet and also showed that the entrainment process is dominated by small-scale eddies near the T/NT interface.[4–6] Holzner *et al.* conducted experiments on oscillating-grid turbulence by using particle tracking velocimetry and investigated the acceleration of fluid particles, the enstrophy, and the rate of strain near the T/NT interface.[15,16] They showed that the viscous process plays an important role in the propagation of the T/NT interface.[17] The importance of small scales in the entrainment was also shown by Taveira *et al.*,[18] in which the trajectory of fluid particles is analyzed using DNS of a temporally developing jet. Recently, the rapid distortion theory has also been used to investigate the T/NT interface.[19]

The turbulent region spreads into the non-turbulent region by conversion of non-turbulent flows near the T/NT interface into turbulent flows. Because the turbulent region is characterized by high enstrophy, the enstrophy transport mechanism near the T/NT interface is important in turbulent region development. The T/NT interface is often detected using a passive scalar when the Schmidt number is large, as shown in previous experiments. Therefore, the dynamics of the T/NT interface is expected to be related to the scalar transport near the interface.

In the present work, the enstrophy and passive scalar transports near the T/NT interface are investigated by using the DNS results of a spatially developing planar jet[20] to elucidate their dominant mechanism. As indicated by Hunt *et al.*,[21] the transport of these physical quantities relative to the T/NT interface is important. First, we derive a transport equation for the enstrophy and the passive scalar in a local coordinate system moving with the T/NT interface. The conditional average of the transport equation for physical quantities (e.g., the turbulent kinetic energy, rate of strain, and enstrophy) is often used to understand the mechanism that dominates these quantities near the T/NT interface.[13,16] The conditional average of the advection term in a coordinate system whose origin is fixed in a flow field indicates how the physical quantities are changed at a fixed location by the advection term before or after the T/NT interface passes the location. Therefore, the conditional average of the advection term in a fixed coordinate system is not useful for investigating the advection relative to the T/NT interface movement, which is expected to be important near the T/NT interface. Analysis in a local coordinate system moving with the T/NT interface enables us to investigate the advection relative to the T/NT interface movement. Finally, we will show that the propagation of the T/NT interface plays an important role in the scalar transport across the interface.

We also focus on the effect of the orientation of the T/NT interface on its characteristics. Bisset *et al.*[8] calculated the conditional mean vorticity, velocity, and passive scalar (temperature) for different interface orientations and interface heights, and showed that the interface orientation has a small effect on these conditional mean values. However, the factors that affect the interface characteristics, such as the interface orientation or height, remain unknown. In addition to the conditional mean values, in this work, we investigate the enstrophy and passive scalar transport mechanism near the T/NT interface for different interface orientations. We will show that they

depend significantly on the interface orientation. Section II describes the DNS of the planar jet. In Sec. III, we derive the transport equation for the enstrophy and passive scalar in a local coordinate system moving with the T/NT interface and consider the role of interface propagation in scalar transport. The numerical results are shown in Sec. IV. Finally, the conclusion is summarized in Sec. V.

II. DIRECT NUMERICAL SIMULATION OF A PLANAR JET

A. Numerical methods and computational parameters

The DNS results for a planar jet[20] are used to investigate the T/NT interface. The numerical methods and simulation conditions are described here. In this work, we consider passive scalar transport in the incompressible planar jet illustrated in Fig. 1. The origin of the coordinate system is located at the center of the jet exit. The streamwise, lateral, and spanwise directions are represented by x, y, and z, respectively. The governing equations are the continuity equation, Navier–Stokes equations, and transport equation for a passive scalar ϕ, which are written as follows:

$$\frac{\partial U_j}{\partial x_j} = 0, \tag{1}$$

$$\frac{\partial U_i}{\partial t} + \frac{\partial U_j U_i}{\partial x_j} = -\frac{\partial p}{\partial x_i} + \nu \frac{\partial^2 U_i}{\partial x_j \partial x_j}, \tag{2}$$

$$\frac{\partial \phi}{\partial t} + \frac{\partial U_j \phi}{\partial x_j} = D \frac{\partial^2 \phi}{\partial x_j \partial x_j}, \tag{3}$$

where U_i is the instantaneous velocity component, p is the instantaneous pressure divided by the density, ν is the kinematic viscosity, and D is the diffusivity coefficient for the passive scalar ϕ.

The governing equations are solved using a finite difference method. The fully conservative fourth-order central difference scheme proposed by Morinishi *et al.*[22] is used for spatial discretization in the x and z directions, and the fully conservative second-order central difference scheme[22] is used in the y direction. The continuity equation and Navier–Stokes equations are solved using the fractional step method. The Poisson equation is solved by the conjugate gradient method. The Crank–Nicolson method is used for the time integration of the y direction viscous and molecular diffusion terms, whereas the other terms are temporally integrated by the third-order Runge–Kutta method. The Crank–Nicolson method is used for preventing the numerical instability arising from the viscous and molecular diffusion terms. This hybrid implicit/explicit scheme was proposed and used in Spalart *et al.*[23] The size of the computational domain is $L_x \times L_y \times L_z = 13.5\pi d \times 11.0\pi d \times 2.6\pi d$, and $N_x \times N_y \times N_z = 700 \times 430 \times 74$ computational grid points are used. The grid is equidistant in the x and z directions. In the y direction, a fine grid is used near the jet centerline. The minimum

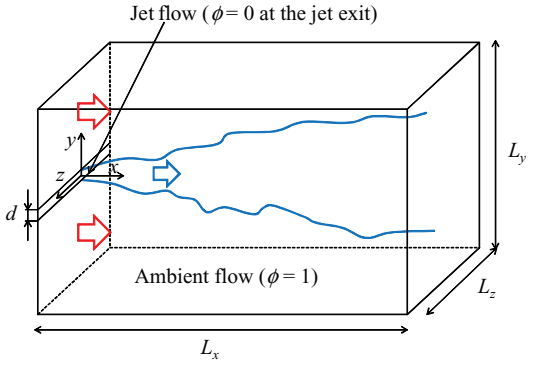

FIG. 1. Planar jet with passive scalar transport.

TABLE I. Coefficients in Eqs. (4) and (5) used to determine boundary condition at jet exit.

n	0	1	2	3	4	5
A_n	1.303×10^{0}	-9.236×10^{-1}	-8.571×10^{0}	-1.207×10^{2}	3.464×10^{2}	0
$B_{u,n}$	4.673×10^{-2}	5.470×10^{-2}	-1.368×10^{0}	1.043×10^{1}	-1.657×10^{1}	0
$B_{v,n}$	3.505×10^{-2}	-1.558×10^{-2}	5.192×10^{-1}	-1.249×10^{0}	0	0
$B_{w,n}$	3.505×10^{-2}	-3.551×10^{-3}	1.930×10^{-1}	-1.186×10^{0}	7.355×10^{0}	-1.267×10^{1}

resolution in the y direction is $0.039d$ on the jet centerline, and maximum resolution is $0.52d$ at $y = \pm L_y/2$, which is far away from the jet. We set the boundary condition of ϕ so that $\phi = 0$ at the jet exit and $\phi = 1$ in the ambient flow. Therefore, the mixture fraction ξ, which is often used as the passive scalar in the jet, is related to ϕ by $\xi = 1 - \phi$. The Reynolds number based on the width of the jet exit d and the mean velocity at the jet exit U_J is $Re = U_J d/\nu = 2,200$, and the Schmidt number for the passive scalar ϕ is $Sc = \nu/D = 1$. The mean streamwise velocity of the ambient flow at $x = 0$ is $U_A = 0.056U_J$. The convective boundary condition[24] is applied to the y–z plane at $x = L_x$. The cross-streamwise gradient of velocity is set to 0 at the lateral boundaries, and the periodic boundary condition is applied in the spanwise direction. We use the measured mean velocity and rms value of the streamwise velocity fluctuation at the jet exit[25–28] to determine the boundary condition. The inflow velocity at the jet exit is generated by superimposing random fluctuations on the mean velocity so that the lateral profiles of the streamwise mean velocity (U_{in}) and the rms values of the velocity fluctuations (u_{rms}, v_{rms}, w_{rms}) at the jet exit satisfy the following equations:

$$\frac{U_{in}(y) - U_A}{U_J} = \sum_{n=0}^{5} A_n \left(\frac{y}{d}\right)^{2n}, \tag{4}$$

$$\frac{u_{rms}(y)}{U_J} = \sum_{n=0}^{5} B_{u,n} \left|\frac{y}{d}\right|^{n}, \frac{v_{rms}(y)}{U_J} = \sum_{n=0}^{5} B_{v,n} \left|\frac{y}{d}\right|^{n}, \frac{w_{rms}(y)}{U_J} = \sum_{n=0}^{5} B_{w,n} \left|\frac{y}{d}\right|^{n}. \tag{5}$$

The coefficients A_n, $B_{u,n}$, $B_{v,n}$, and $B_{w,n}$, are summarized in Table I. The measurement results[25–28] for $U_{in}(y)$ and $u_{rms}(y)$ are compared with Eqs. (4) and (5) in Fig. 2. Equations (4) and (5) are used to generate the inflow velocity, which is similar to that in the experiments.[25–28] The profiles of the mean velocity and the rms value of the streamwise velocity fluctuation at the jet exit used in the present DNS are similar to those in turbulent channel flows. Therefore, the coefficients $B_{v,n}$ and $B_{w,n}$ are determined from the profiles of v_{rms} and w_{rms} in the turbulent channel flow.[29] Thus, the inflow velocity used in the present DNS approximates the velocity profile in the jet nozzle rather than near the jet exit. In the ambient flow at $x = 0$, the streamwise velocity is set to U_A without any fluctuations.

B. Validations of the DNS results

To validate the DNS results, the conventional statistics obtained by the present DNS are compared with the previous experiments and DNSs on planar jets. The term "conventional statistics" denotes the statistics obtained by time averaging or ensemble averaging procedures. Here, the mixture fraction $\xi = 1 - \phi$ is used instead of ϕ. In the present DNS, the inflow velocity profiles are determined according to the experiment on the planar liquid jet in Watanabe *et al.*[25–28] The streamwise and cross-streamwise velocities statistics obtained in the present DNS are compared with those measured by the X-type hot-film probe in the planar liquid jet. In the experiment by Watanabe *et al.*,[25–28] the mixture fraction was also measured for $Sc = 600$. The mean mixture fraction profile is determined by its transport by the velocity and the molecular diffusion. In the jet flow, the velocity field has much greater influence on the mean mixture fraction profile than the molecular diffusion, and the mean molecular diffusion term is often neglected in the mean scalar transport

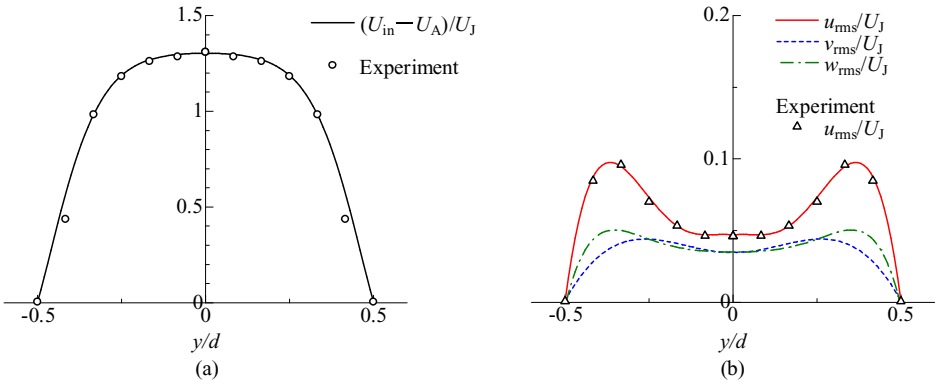

FIG. 2. (a) Mean streamwise velocity and (b) rms values of velocity fluctuations at jet exit. Lateral profiles of velocity statistics at jet exit are compared with measurement results.[25–28]

equation.[30] The difference in the Schmidt number significantly affects the molecular diffusion, and can be neglected in the mean mixture fraction profile. Therefore, although there is a discrepancy in the Schmidt number, it is adequate that the mean mixture fraction profile is compared between the DNS and the experiments in the liquid jet.

Figures 3(a) and 3(b) show the mean streamwise velocity $\langle U\rangle$ and mean mixture fraction $\langle\xi\rangle$ on the jet centerline. Here, $\langle\ \rangle$ denotes the conventional mean value. The results show that the streamwise development of the mean streamwise velocity and mean mixture fraction agrees well with the experimental results. It is also found that $\langle U\rangle - U_A$ and $\langle\xi\rangle$ on the jet centerline decrease with proportion to $(x/d)^{-1/2}$. In the downstream of $x/d = 10$, the mean streamwise velocity and mean mixture fraction on the jet centerline change according to

$$\frac{U_J^2}{(\langle U\rangle - U_A)^2} = 0.132(x/d) + 0.125, \tag{6}$$

$$\frac{1}{\langle\xi\rangle^2} = 0.199(x/d) + 0.549. \tag{7}$$

Figures 4(a) and 4(b) show the lateral profiles of the mean streamwise velocity and the mean mixture fraction. The cross-streamwise coordinate y is normalized by the jet half-widths b_U and b_ξ based on the lateral profiles of $(\langle U\rangle - U_A)$ and $\langle\xi\rangle$, respectively. The mean streamwise velocity and the mean mixture fraction are normalized by their values on the jet centerline. Here, $\langle\ \rangle_C$ denotes the conventional mean value on the jet centerline. Both the mean streamwise velocity and the mean mixture fraction exhibit self-similar profiles, and show good agreement with the experimental results in the liquid jet.[25–28]

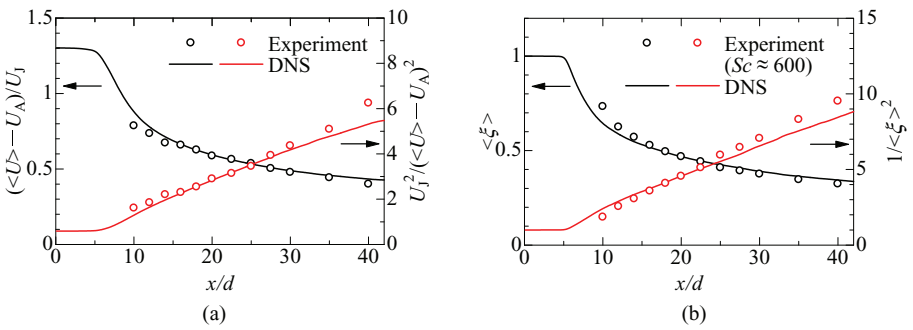

FIG. 3. Streamwise variation in mean streamwise velocity and mean mixture fraction on jet centerline. (a) Mean streamwise velocity. (b) Mean mixture fraction. The experiments by Watanabe *et al.*[25,28] are compared with the present DNS.

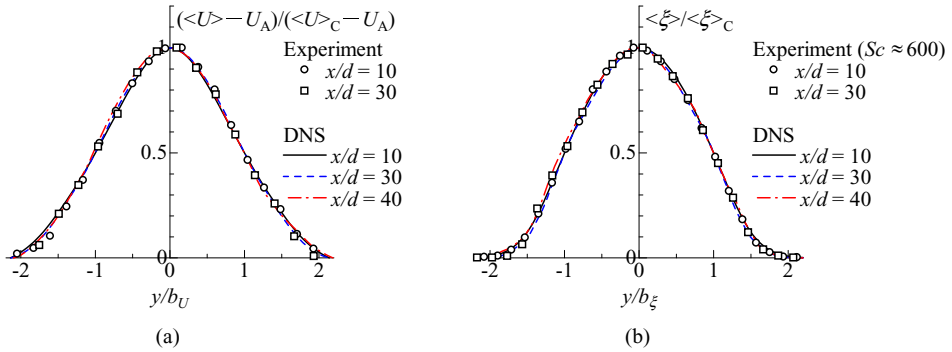

FIG. 4. Lateral profiles of mean values of (a) streamwise velocity and (b) mixture fraction. The experiments by Watanabe *et al.*[25,28] are compared with the present DNS.

Figure 5 shows the streamwise variation in the jet half-widths b_U and b_ξ. Similar to the experiments,[25,28] b_U and b_ξ increase with proportion to x. In the downstream of $x/d = 10$, b_U and b_ξ change according to

$$b_U/d = 0.079(x/d) + 0.263, \tag{8}$$

$$b_\xi/d = 0.118(x/d) + 0.230. \tag{9}$$

Thus, the mean mixture fraction more rapidly spreads in the y direction than the mean streamwise velocity.

The development of the mean velocity and scalar fields strongly depends on the inflow velocity.[31,32] The inflow velocity generated by random fluctuations is different from real turbulence. However, the agreement in the mean fields between the DNS and the experiments justifies the application of the random fluctuations as the inflow velocity for the planar jet investigated in this study.

Figures 6(a) and 6(b) show the lateral profiles of the rms values of the streamwise and cross-streamwise velocity fluctuations ($u_{\rm rms}$, $v_{\rm rms}$) normalized by $\langle U\rangle_C - U_A$. The results obtained in the previous experiments[25,28,33,34] and DNSs[35,36] are also shown in Fig. 6. Although there is variability among the experiments and the DNSs, the profiles obtained by the present DNS are similar to those in the previous studies. It should be noted that the rms values agree well with the experimental results by Watanabe *et al.*[25,28]

Figure 7 shows the lateral profiles of the rms values of mixture fraction fluctuation, $\xi_{\rm rms}$, normalized by the mean mixture fraction $\langle\xi\rangle_C$ on the jet centerline. The measurement results of temperature by Davies *et al.*[37] and concentration of diffusive dye by Watanabe *et al.*[25,28] are also shown in this figure. Because the dissipation of scalar fluctuations occurs in small scales, where the molecular diffusion is important, the Schmidt number can affect $\xi_{\rm rms}$. However, comparison

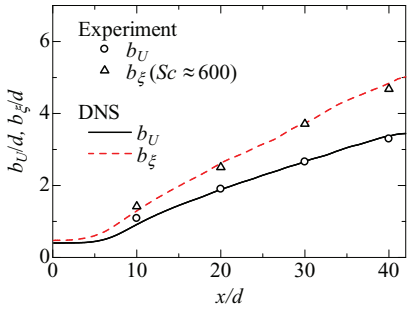

FIG. 5. Jet half-width based on mean streamwise velocity and mean mixture fraction. The experiments by Watanabe *et al.*[25,28] are compared with the present DNS.

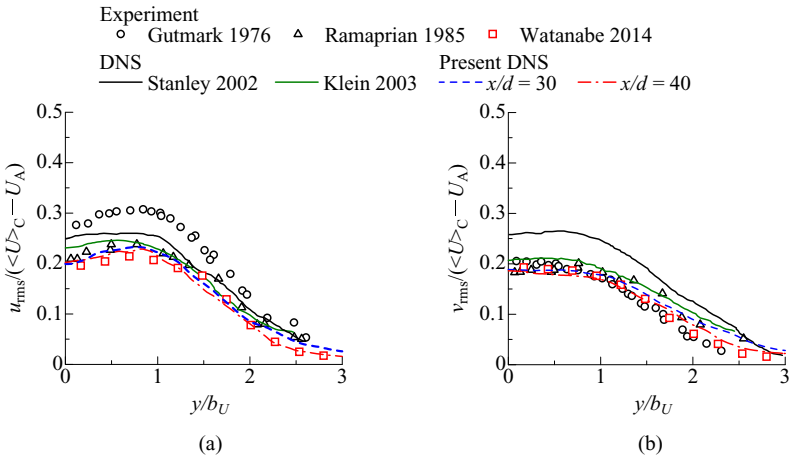

FIG. 6. Lateral profiles of rms values of (a) streamwise velocity fluctuation and (b) cross-streamwise velocity fluctuation. The experiments by Gutmark and Wygnansk,[33] Ramaprian and Chandrasekhara,[34] and Watanabe *et al.*[25,28] and the DNSs by Stanley *et al.*[35] and Klein *et al.*[36] are compared with the present DNS.

between the DNS and the experiments is still useful for investigating the overall profile of $\xi_{\rm rms}$. $\xi_{\rm rms}/\langle\xi\rangle_{\rm C}$ measured by Davies *et al.* is small compared with the present DNS and the experiments on the planar liquid jet by Watanabe *et al.* Although a large difference in $\xi_{\rm rms}/\langle\xi\rangle_{\rm C}$ can be observed at $x/d = 10$ between the present DNS and the experiments by Watanabe *et al.*, $\xi_{\rm rms}/\langle\xi\rangle_{\rm C}$ shows good agreement in the downstream region.

Figure 8 shows the spectrum of the streamwise velocity fluctuation and the mixture fraction fluctuation at $(x, y) = (30d, 0.7b_U)$. In this figure, the spectrum is normalized by the variances of the streamwise velocity fluctuation and the mixture fraction fluctuation. In Fig. 8(a), the wavenumber $2\pi f/\langle U\rangle$ obtained from the frequency f is normalized by the Kolmogorov wavenumber $1/\eta_{\rm K} = (\epsilon/\nu^3)^{1/4}$, where $\epsilon = 2\nu\langle s_{ij}s_{ij}\rangle$ is the mean dissipation rate of the turbulent kinetic energy (s_{ij} is the fluctuating rate of strain tensor). In Fig. 8(b), the wavenumber corresponding to the Batchelor scale $1/\eta_{\rm B} = Sc^{1/2}/\eta_{\rm K}$ is used to normalize the wavenumber. It is found that there is a band of frequencies where E_{uu} and $E_{\xi\xi}$ exhibit power laws with an exponent close to $-5/3$. The spectrum at the high frequency shows that the velocity and mixture fraction fluctuations at small scales are well resolved by the present DNS.

Compared with the previous DNSs of the spatially developing planar jets,[35,36] the present DNS has a small spatial resolution relative to the Kolmogorov microscale especially in the downstream region, where the detail analysis is conducted on the T/NT interface in this study. We have also confirmed that the spatial resolution is small enough to investigate the enstrophy and passive scalar transport near the interface. An additional DNS with a higher spatial resolution was conducted

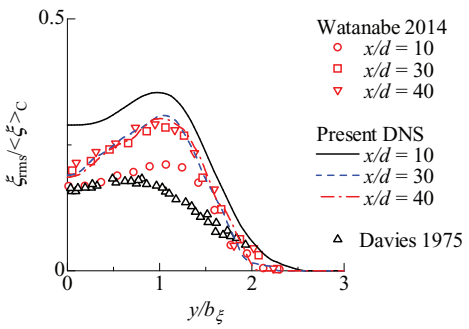

FIG. 7. Lateral profiles of rms values of mixture fraction fluctuation. The experiments by Davies *et al.*[37] and Watanabe *et al.*[25,28] are compared with the present DNS.

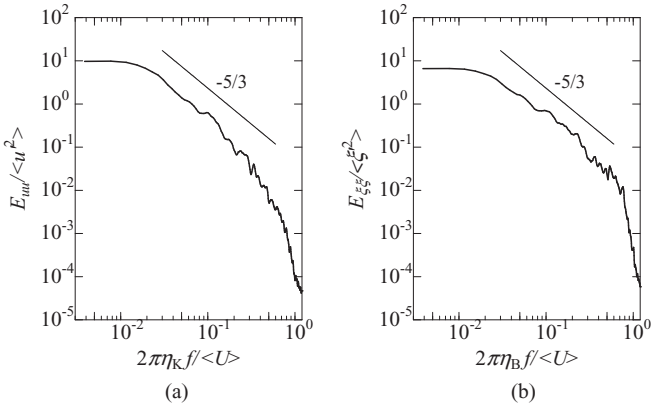

FIG. 8. Spectrum of the streamwise velocity fluctuation and the mixture fraction fluctuation at $(x, y) = (30d, 0.7b_U)$. (a) Streamwise velocity fluctuation. (b) Mixture fraction fluctuation.

(fine-grid DNS). The numerical methods in the fine-grid DNS are almost similar to those in the present DNS in this paper, and are shown in Watanabe *et al.*[20,38] Comparing the results of analysis on the enstrophy transport near the T/NT interface between the two DNSs, we confirmed that the spatial resolution in the present DNS is small enough. The computational domain in the fine-grid DNS is small compared with the present DNS owing to the limitation of computer resources. For analyzing the fully developed region of the planar jet, we used the present DNS instead of the fine-grid DNS.

III. LOCAL COORDINATE SYSTEM MOVING WITH THE T/NT INTERFACE

A. Enstrophy transport equation in the local coordinate system moving with the T/NT interface

The interface movement should be taken into account when analyzing the characteristics of the T/NT interface. In this section, the transport equations for the enstrophy and passive scalar in the local coordinate system moving with the T/NT interface are derived. The enstrophy transport equation is used to derive the propagation velocity of the T/NT interface. Then, we analyze the scalar transport near the T/NT interface.

We introduce a coordinate system whose origin is located at the T/NT interface. This coordinate system is referred to as the "local coordinate system" hereafter, whereas the coordinate system whose origin is located at a fixed location in a flow field, such as a jet exit, is referred to as the "fixed coordinate system." The positions in the fixed and local coordinate systems are represented by $\mathbf{x}$ and $\mathbf{x}^{\mathrm{I}}$, respectively. The relationship between the fixed and local coordinate systems is illustrated in Fig. 9. The point $\mathbf{x} = \mathbf{x}_0^{\mathrm{I}}$ is located on the T/NT interface and is used as the origin of the local coordinate system. We use $\mathbf{U}(\mathbf{x})$ to represent the velocity of the fluid at $\mathbf{x}$ in the fixed coordinate system. Note that the velocity in the local coordinate system is not consistent with $\mathbf{U}$ because of the T/NT interface movement. According to Holzner and Lüthi,[17] the velocity of the T/NT interface movement $\mathbf{U}^{\mathrm{I}}$ can be divided into two components. One is the velocity of the fluid at $\mathbf{x} = \mathbf{x}_0^{\mathrm{I}}$, and the other is the velocity of the T/NT interface relative to the velocity of the fluid at $\mathbf{x} = \mathbf{x}_0^{\mathrm{I}}$, which is referred to as propagation velocity. Hence, the velocity of the T/NT interface movement $\mathbf{U}^{\mathrm{I}}$ is represented by

$$\mathbf{U}^{\mathrm{I}} = \mathbf{U}(\mathbf{x}_0^{\mathrm{I}}) + \mathbf{V}^{\mathrm{P}}, \tag{10}$$

where $\mathbf{V}^{\mathrm{P}}$ denotes the propagation velocity of the T/NT interface.

We consider the coordinate transformation from the fixed coordinate system $(\mathbf{x}, t)$ to the local coordinate system $(\mathbf{x}^{\mathrm{I}}, t')$. Here, the local coordinate system $(\mathbf{x}^{\mathrm{I}}, t')$ is related to the fixed coordinate

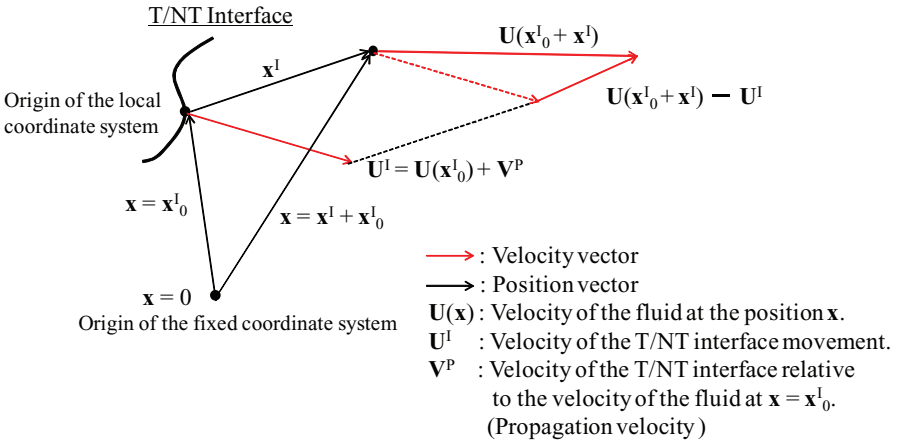

FIG. 9. Relationship between fixed and local coordinate systems.

system ($\mathbf{x}$, t) by

$$\mathbf{x} = \mathbf{x}^{\mathrm{I}}_0 + \mathbf{x}^{\mathrm{I}}, \tag{11}$$

$$t = t'. \tag{12}$$

Because the origin of the local coordinate system moves with the velocity $\mathbf{U}^{\mathrm{I}}$, we can obtain the following relationship from Eq. (11):

$$\frac{\partial \mathbf{x}^{\mathrm{I}}_0}{\partial t} = -\frac{\partial \mathbf{x}^{\mathrm{I}}}{\partial t} = \mathbf{U}^{\mathrm{I}}. \tag{13}$$

Then, the derivative of the variable $f = f(\mathbf{x}^{\mathrm{I}}, t')$ with respect to t is written as follows:

$$\frac{\partial f}{\partial t} = \frac{\partial f}{\partial t'}\frac{\partial t'}{\partial t} + \frac{\partial f}{\partial x^{\mathrm{I}}_i}\frac{\partial x^{\mathrm{I}}_i}{\partial t}, \tag{14}$$

$$= \frac{\partial f}{\partial t'} - U^{\mathrm{I}}_i \frac{\partial f}{\partial x^{\mathrm{I}}_i}. \tag{15}$$

Here, x^{I}_i and U^{I}_i are the i direction components of $\mathbf{x}^{\mathrm{I}}$ and $\mathbf{U}^{\mathrm{I}}$, respectively. Similarly, the derivative of $f = f(\mathbf{x}^{\mathrm{I}}, t')$ with respect to x_i is written as follows:

$$\frac{\partial f}{\partial x_i} = \frac{\partial f}{\partial t'}\frac{\partial t'}{\partial x_i} + \frac{\partial f}{\partial x^{\mathrm{I}}_j}\frac{\partial x^{\mathrm{I}}_j}{\partial x_i}, \tag{16}$$

$$= \frac{\partial f}{\partial x^{\mathrm{I}}_i}. \tag{17}$$

Here, x_i is the i direction component of $\mathbf{x}$. By using Eqs. (15) and (17), the Lagrangian derivative of f at $\mathbf{x} = \mathbf{x}^{\mathrm{I}}_0 + \mathbf{x}^{\mathrm{I}}$ can be represented in the local coordinate system ($\mathbf{x}^{\mathrm{I}}$, t') as follows:

$$\frac{Df}{Dt} = \frac{\partial f}{\partial t} + U_i(\mathbf{x}^{\mathrm{I}} + \mathbf{x}^{\mathrm{I}}_0)\frac{\partial f}{\partial x_i}, \tag{18}$$

$$= \frac{\partial f}{\partial t'} - U^{\mathrm{I}}_i \frac{\partial f}{\partial x^{\mathrm{I}}_i} + U_i(\mathbf{x}^{\mathrm{I}} + \mathbf{x}^{\mathrm{I}}_0)\frac{\partial f}{\partial x^{\mathrm{I}}_i}, \tag{19}$$

$$= \frac{\partial f}{\partial t'} + \left(U_i(\mathbf{x}^{\mathrm{I}} + \mathbf{x}^{\mathrm{I}}_0) - U^{\mathrm{I}}_i\right)\frac{\partial f}{\partial x^{\mathrm{I}}_i}. \tag{20}$$

Additionally, the following expression for the Lagrangian derivative in the local coordinate system can be obtained using Eq. (17):

$$\frac{Df}{Dt} = \frac{\partial f}{\partial t'} + \left(U_i(\mathbf{x}^{\mathrm{I}} + \mathbf{x}_0^{\mathrm{I}}) - U_i^{\mathrm{I}}\right) \frac{\partial f}{\partial x_i}, \tag{21}$$

$$= \frac{\partial f}{\partial t'} + \left(\mathbf{U}(\mathbf{x}^{\mathrm{I}} + \mathbf{x}_0^{\mathrm{I}}) - \mathbf{U}^{\mathrm{I}}\right) \cdot \nabla f. \tag{22}$$

Equation (21) or (22) is useful for investigating the T/NT interface because the advection term can be evaluated using the derivative in the fixed coordinate system. In Eq. (22), the velocity in the advection term represents the velocity at $\mathbf{x} = \mathbf{x}^{\mathrm{I}} + \mathbf{x}_0^{\mathrm{I}}$ relative to the velocity of the T/NT interface movement, as shown in Fig. 9. Substituting Eq. (10) into Eq. (22) yields the following expression for the Lagrangian derivative in the local coordinate system:

$$\frac{Df}{Dt} = \frac{\partial f}{\partial t'} + \left(\mathbf{U}(\mathbf{x}^{\mathrm{I}} + \mathbf{x}_0^{\mathrm{I}}) - \mathbf{U}(\mathbf{x}_0^{\mathrm{I}}) - \mathbf{V}^{\mathrm{P}}\right) \cdot \nabla f. \tag{23}$$

The propagation velocity $\mathbf{V}^{\mathrm{P}}$ has to be specified to evaluate the advection term in Eq. (23). Holzner and Lüthi derived the expression for $\mathbf{V}^{\mathrm{P}}$ by analyzing the enstrophy transport equation in the fixed coordinate system.[17] We can derive the same expression for $\mathbf{V}^{\mathrm{P}}$ from the transport equation for the enstrophy $(\omega^2/2)$ in the local coordinate system, which can be derived by using Eq. (23),

$$\frac{\partial \omega^2/2}{\partial t'} = -\left(\mathbf{U}(\mathbf{x}^{\mathrm{I}} + \mathbf{x}_0^{\mathrm{I}}) - \mathbf{U}(\mathbf{x}_0^{\mathrm{I}}) - \mathbf{V}^{\mathrm{P}}\right) \cdot \nabla(\omega^2/2) + \omega_i \omega_j S_{ij} + \nu \omega_i \nabla^2 \omega_i. \tag{24}$$

Here, $\omega_i = \epsilon_{ijk} \partial U_j / \partial x_k$ is the i direction component of the vorticity vector (where ϵ_{ijk} is the Levi-Civita symbol), and $S_{ij} = (\partial U_i/\partial x_j + \partial U_j/\partial x_i)/2$ is the component of the rate of strain tensor. The first term on the right-hand side of Eq. (24) is the advection term, the second term is the production term, and the third term is the viscous term. When the vorticity magnitude $|\boldsymbol{\omega}|$ is used to detect the T/NT interface, the detected interface is the isosurface of $|\boldsymbol{\omega}|$. Therefore, the enstrophy $(\omega^2/2)$ at the T/NT interface $(\mathbf{x}^{\mathrm{I}} = 0)$ does not change with time,

$$\frac{\partial \omega^2/2}{\partial t'} = \mathbf{V}^{\mathrm{P}} \cdot \nabla(\omega^2/2) + \omega_i \omega_j S_{ij} + \nu \omega_i \nabla^2 \omega_i = 0. \tag{25}$$

Because the propagation velocity $\mathbf{V}^{\mathrm{P}}$ points in the direction normal to the T/NT interface, $\mathbf{V}^{\mathrm{P}}$ is represented by

$$\mathbf{V}^{\mathrm{P}} = v_{\mathrm{n}} \mathbf{n} = v_{\mathrm{n}} \frac{-\nabla \omega^2}{|\nabla \omega^2|}, \tag{26}$$

where $\mathbf{n} = -\nabla\omega^2/|\nabla\omega^2|$ is the unit vector normal to the T/NT interface, and v_{n} is the propagation velocity component normal to the T/NT interface. Here, v_{n} is defined as positive when the T/NT interface propagates toward the non-turbulent region and as negative when the T/NT interface propagates toward the turbulent region. By substituting Eq. (26) into Eq. (25), we can derive the propagation velocity v_{n} as

$$v_{\mathrm{n}} = \frac{2\omega_i \omega_j S_{ij}}{|\nabla \omega^2|} + \frac{2\nu \omega_i \nabla^2 \omega_i}{|\nabla \omega^2|} = v_{\mathrm{P}} + v_{\mathrm{Vis}}. \tag{27}$$

Equation (27) is the same as the propagation velocity derived by Holzner and Lüthi.[17] The first term in Eq. (27) is the propagation velocity arising from enstrophy production or destruction, and the second term is the propagation velocity arising from the viscous effects. The viscous term in the enstrophy transport equation can be decomposed into the viscous diffusion term and the viscous dissipation term, and the enstrophy transport equation is represented by

$$\frac{\partial \omega^2/2}{\partial t'} = -\left(\mathbf{U}(\mathbf{x}^{\mathrm{I}} + \mathbf{x}_0^{\mathrm{I}}) - \mathbf{U}(\mathbf{x}_0^{\mathrm{I}}) - \mathbf{V}^{\mathrm{P}}\right) \cdot \nabla(\omega^2/2)$$
$$+\omega_i \omega_j S_{ij} + \nu \nabla^2(\omega^2/2) - \nu \nabla \omega_i \cdot \nabla \omega_i. \tag{28}$$

The third and fourth terms in Eq. (28) are the viscous diffusion term and viscous dissipation term, respectively. When this decomposition of the viscous term is applied to Eq. (27), the propagation velocity v_n is represented by

$$v_n = \frac{2\omega_i\omega_j S_{ij}}{|\nabla\omega^2|} + \frac{2\nu\nabla^2(\omega^2/2)}{|\nabla\omega^2|} - \frac{2\nu\nabla\omega_i\cdot\nabla\omega_i}{|\nabla\omega^2|} = v_P + v_D + v_\epsilon. \tag{29}$$

Here, v_D is the propagation velocity arising from viscous diffusion, and v_ϵ is that arising from viscous dissipation.

B. Scalar transport equation in the local coordinate system moving with the T/NT interface

We analyze the scalar transport near the T/NT interface. Here, we consider the passive scalar ϕ, whose spatial and temporal evolution is given by Eq. (3). In the local coordinate system, the transport equation for ϕ is written as follows:

$$\frac{\partial\phi}{\partial t'} = -\left(\mathbf{U}(\mathbf{x}^I + \mathbf{x}_0^I) - \mathbf{U}(\mathbf{x}_0^I) - \mathbf{V}^P\right)\cdot\nabla\phi + D\nabla^2\phi. \tag{30}$$

Using Eq. (30) instead of Eq. (3) enables us to analyze the scalar transport across the T/NT interface. At the T/NT interface ($\mathbf{x}^I = 0$), the scalar ϕ changes according to

$$\frac{\partial\phi}{\partial t'} = \mathbf{V}^P\cdot\nabla\phi + D\nabla^2\phi, \tag{31}$$

$$= \nabla\cdot(\phi\mathbf{V}^P) + D\nabla^2\phi. \tag{32}$$

Here $\mathbf{V}^P\cdot\nabla\phi = \nabla\cdot(\phi\mathbf{V}^P)$ is used to derive Eq. (32). Here, because v_n is independent of x_n, this relationship can be obtained by

$$\mathbf{V}^P\cdot\nabla\phi = v_n\mathbf{n}\cdot\nabla\phi = v_n\frac{\partial\phi}{\partial x_n} = \frac{\partial v_n\phi}{\partial x_n} = \nabla\cdot\mathbf{n}(v_n\phi) = \nabla\cdot(\phi\mathbf{V}^P), \tag{33}$$

where x_n is the normal direction to the interface.

For further understanding of the role of the term $\nabla\cdot(\phi\mathbf{V}^P)$ in the scalar entrainment process, we consider a one-dimensional coordinate system, where the position in the fixed coordinate system is represented by y. The local coordinate $\mathbf{x}_I$ consists of one component, i.e., the distance from the T/NT interface y_I. Here, the non-turbulent region corresponds to positive y_I, and the turbulent region corresponds to negative y_I. Figure 10 shows the y_I direction profile of ϕ near the T/NT interface. The interface positions at $t = t_0$ and $t = t_0 + \Delta t$ are represented by y_1 and y_2, respectively. The profile of ϕ is similar to that in the present DNS, in which $\phi = 1$ in the ambient (irrotational) flow. For simplicity, the profile of ϕ is assumed not to change during the time interval Δt, whereas the T/NT interface propagates toward the non-turbulent region. Under this assumption, $\nabla\cdot(\phi\mathbf{V}^P)$ is the only term that causes ϕ to change. As shown in Fig. 10, during Δt, the T/NT interface moves toward the non-turbulent region, where ϕ is larger than the value at the position where the T/NT interface is located at $t = t_0$, and the region between y_1 and y_2 becomes turbulent. The value of ϕ at the T/NT

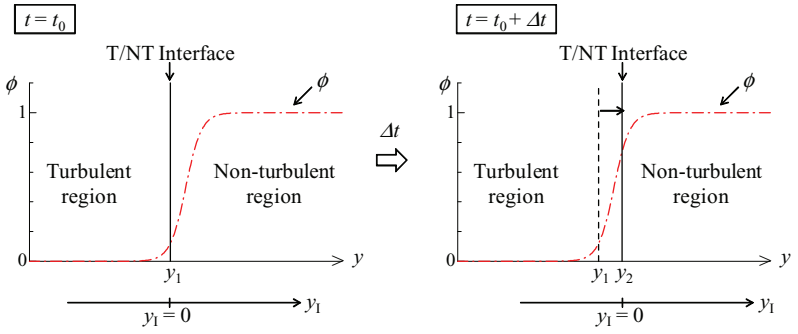

FIG. 10. Role of interface propagation in scalar transport across T/NT interface.

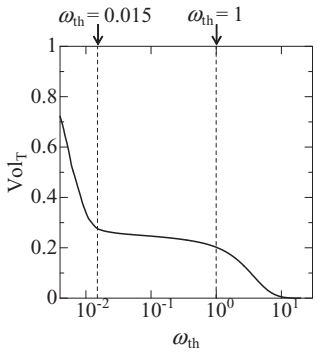

FIG. 11. Volume fraction of turbulent region as a function of threshold ω_{th}.

interface is increased by interface propagation toward the turbulent region. The temporal variation in ϕ at the T/NT interface caused by interface propagation is represented by $\nabla \cdot (\phi \mathbf{V}^P)$. As a result of interface propagation, the scalar ϕ between y_1 and y_2 is transported into the turbulent region from the non-turbulent region across the T/NT interface. In this case, $\phi \mathbf{V}^P$ represents the scalar flux corresponding to this scalar transport across the T/NT interface. Thus, interface propagation toward the non-turbulent region causes scalar entrainment and transports the scalar ϕ in the non-turbulent region into the turbulent region across the T/NT interface. In contrast, when the T/NT interface propagates toward the turbulent region in Fig. 10, the scalar ϕ between y_1 and y_2 is left in the non-turbulent region, and the scalar ϕ in the turbulent region is transported to the non-turbulent region across the T/NT interface.

IV. RESULTS AND DISCUSSION

A. Detection of the T/NT interface

The vorticity magnitude $|\boldsymbol{\omega}|$ is used to detect the T/NT interface, and the region in which $|\boldsymbol{\omega}| b_U / U_C \geq \omega_{th}$ is defined as the turbulent region. Here, U_C is the mean streamwise velocity on the jet centerline. Note that although the vorticity magnitude decays in the streamwise direction, b_U/U_C increases with proportion to $(x/d)^{3/2}$. In Taveira *et al.*,[18] the threshold ω_{th} is determined from the dependence of the volume fraction of the detected turbulent region Vol_T on the threshold. In this study, Vol_T is calculated in the region $x/d \geq 10$, where self-similar profiles can be observed in the mean streamwise velocity and mean mixture fraction. Figure 11 shows the relationship between Vol_T and ω_{th}. As the threshold ω_{th} increases, the turbulent volume decreases, but Vol_T changes slowly for $0.015 \leq \omega_{th} \leq 1$. We choose a threshold value from this range and set $\omega_{th} = 0.7$. The T/NT interface can thus be represented by the isosurface of $|\boldsymbol{\omega}| b_U / U_C = 0.7$. Note that the same interface detection threshold was also used by Bisset *et al.*[8]

We focus on the effect of the orientation on the T/NT interface characteristics. Figure 12 shows a schematic of the T/NT interface in the planar jet, where the interface height is denoted by Y_I. We consider three orientations: the cross-streamwise, leading, and trailing edges, which are distinguished

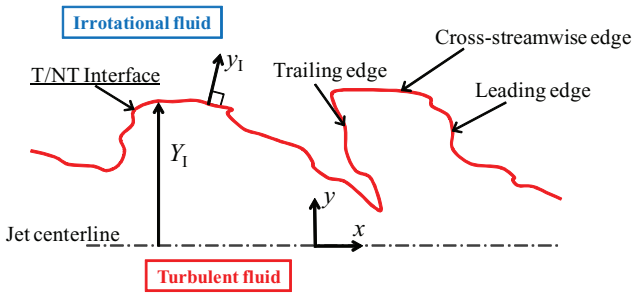

FIG. 12. Schematic of T/NT interface in jet flow and definition of interface orientation.

by **n**. The cross-streamwise edge is defined by **n** being parallel to the y direction. The leading and trailing edges face the downstream and upstream regions, respectively, and are defined by **n** being parallel to the x direction.

The conditional statistics conditioned on the distance from the T/NT interface[8,9] are analyzed using a procedure similar to that in previous work.[38] To calculate the conditional statistics, y_{I} is introduced as shown in Fig. 12 and is normal to the T/NT interface. The turbulent flow is located at $y_{\mathrm{I}} < 0$, whereas the non-turbulent flow is at $y_{\mathrm{I}} > 0$. The conditional statistics conditioned on y_{I} are calculated for the detected T/NT interface defined by the isosurface of the vorticity norm. The conditional averages, denoted by $\langle\ \rangle_{\mathrm{I}}$, are calculated for each interface orientation, and deviations of the interface orientation within $\pm 25^{\circ}$ are accepted. This criterion is the same as that used by Bisset *et al.*[8] and Watanabe *et al.*[38] The angle between **n** and the x or y direction is calculated by taking the inner product of **n** and the relevant unit vector. Although the angle between **n** and the x or y direction may not be zero, y_{I} is set to be parallel to the x or y direction for calculating the conditional statistics for the three interface orientations. To calculate the conditional statistics, variables in the local coordinates are obtained by using the linear interpolation. Because of the simplified definition of y_{I}, the interpolation is performed in one direction, i.e., normal to the interface.

The conditional statistics are calculated on both sides of the T/NT interface, but when the conditional statistics are calculated for a T/NT interface, it is possible that another interface will appear in close proximity. The characteristics of the flow field vary drastically near the T/NT interface, and the width of this variation is close to the Taylor microscale λ. Therefore, if another interface appears, the region within a distance of λ from the interface is not used for calculating the conditional statistics. Here, λ is defined as $(\lambda_x + \lambda_y + \lambda_z)/3$, where $\lambda_i = \sqrt{\langle u_i'^2\rangle / \langle (\partial u_i'/\partial x_i)^2\rangle}$ (in the i direction), and $u_i' = U_i - \langle U_i\rangle$ is the velocity fluctuation. The existence of another interface is examined only in the direction of y_{I}. Bisset *et al.*[8] have shown that the conditional statistics for the interface can be affected by another interface. Restricting the calculation region is particularly important for the leading and trailing edges because these edges often face each other.

The conditional statistics are evaluated at various streamwise locations, and at $x = x_0$, the interface detected in the region of $x_0 - d \le x \le x_0 + d$ is used for the calculations. To obtain converged statistics, 850 instantaneous flow and scalar fields at different time steps are used. The time interval between two instantaneous fields is d/U_{J}, and so the conditional statistics are calculated for a time interval of $850d/U_{\mathrm{J}}$, which is 10.6 times longer than the flow time unit defined by $2L_x/(U_{\mathrm{J}} + U_{\mathrm{A}})$.

The conditional statistics in the turbulent region are calculated upstream of the leading edge and downstream of the trailing edge. Leading and trailing edges detected at almost the same streamwise location are used for the analysis. Thus, the turbulent region near the trailing edge is at a larger x position than that near the leading edge. It should also be noted that as $|y_{\mathrm{I}}|$ decreases the separation in the x direction between the turbulent regions near the two interfaces decreases, and therefore, any differences in the conditional statistics near the interface between the leading and trailing edges can be considered to be caused by the interface characteristics.

Figure 13(a) shows a snapshot of the vorticity field in the x–y plane and the detected T/NT interface (emphasized by the thick white line). The detected T/NT interface is convoluted and envelops a region with a large $|\boldsymbol{\omega}|$. The use of $|\boldsymbol{\omega}| = 0.7U_{\mathrm{C}}/b_U$ as a threshold creates "holes" of non-turbulent flow in the turbulent region and "islands" of turbulent flow in the non-turbulent region, but these have been removed from the figure, and the associated T/NT interfaces are not used for calculating the conditional statistics. Figure 13(b) shows the probability density function (PDF) of the normalized interface height Y_{I}/b_U obtained at different streamwise locations, and we see that the shape of the PDF is almost independent of the streamwise location. The mean T/NT interface height is $1.76b_U$ at $x/d = 38$, the rms value of the fluctuation of Y_{I} is $0.435b_U$, and the skewness and flatness of Y_{I} are -0.0569 and 3.00, respectively. Thus, $p(Y_{\mathrm{I}}/b_U)$ is similar to a Gaussian profile. This has also been observed in previous studies.[6–8] However, although the skewness is small, the PDF of Y_{I}/b_U is negatively skewed, unlike that found in experiments of a round jet.[6]

The T/NT interface in the region of $3L_x/4 \le x \le L_x$ and $y \le 0$ is visualized in Figs. 14 (cross-streamwise edge) and 15 (leading and trailing edges); λ is also shown for reference. We see that

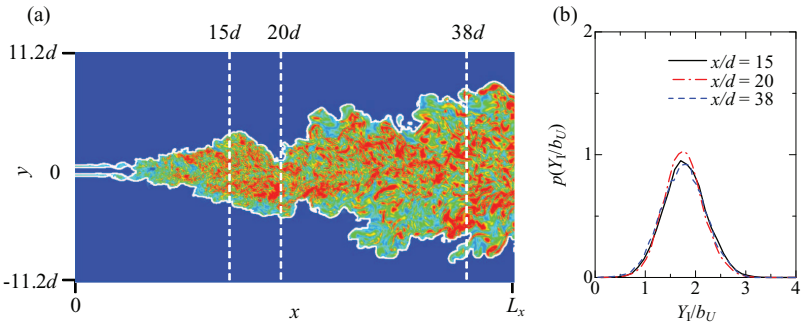

FIG. 13. Detected T/NT interface. (a) Visualization of T/NT interface and vorticity field. White lines represent the T/NT interface. Color contour represents the value of the normalized vorticity magnitude $|\boldsymbol{\omega}|b_U/U_C$. Blue: $|\boldsymbol{\omega}| = 0$. Red: $|\boldsymbol{\omega}| \geq 5U_C/b_U$. The vertical broken lines show the streamwise locations $x/d = 15$, 20, and 38. (b) Probability density function of T/NT interface height Y_I.

while the interface is orientated in various directions because of its convoluted structure the interface orientation is correctly distinguished. There are a larger number of detected cross-streamwise edges than leading and trailing edges; the cross-streamwise, leading, and trailing edges account for 10%, 5%, and 4% of the detected T/NT interface around $x/d = 38$, respectively.

B. Conditional averages of the velocity and the vorticity

Figure 16 shows $\langle|\boldsymbol{\omega}|b_U/U_C\rangle_I$ near the interface detected at $x/d = 20$ and 38. Here, y_I is normalized by λ on the jet centerline because λ is almost independent of the cross-streamwise

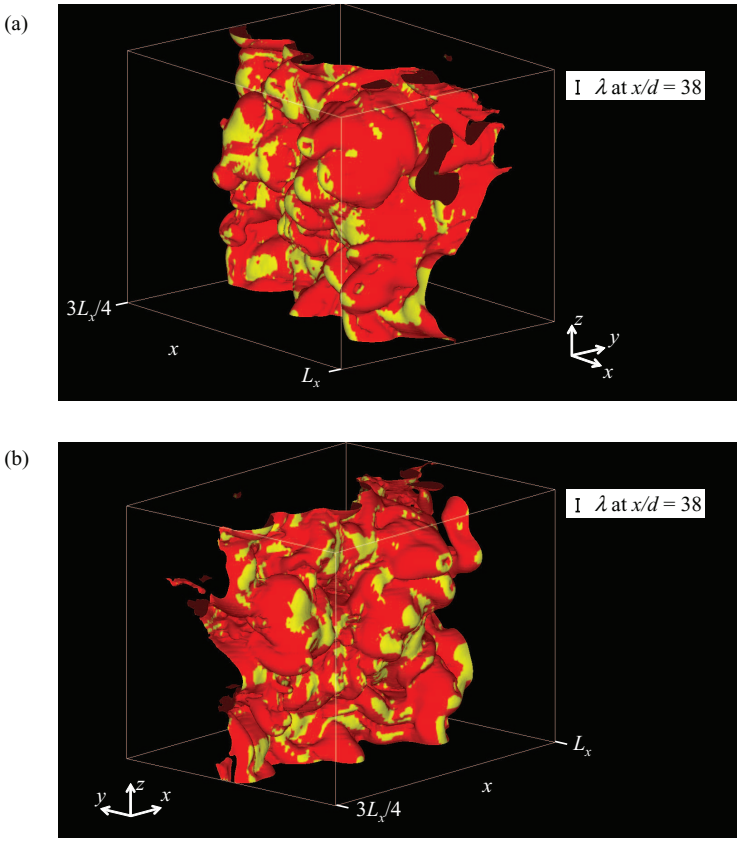

FIG. 14. Three-dimensional visualization of T/NT interface in the region $3L_x/4 \leq x \leq L_x$ and $y \leq 0$. Yellow: cross-streamwise edge. Red: other interface orientations. (a) View from downstream region. (b) View from upstream region.

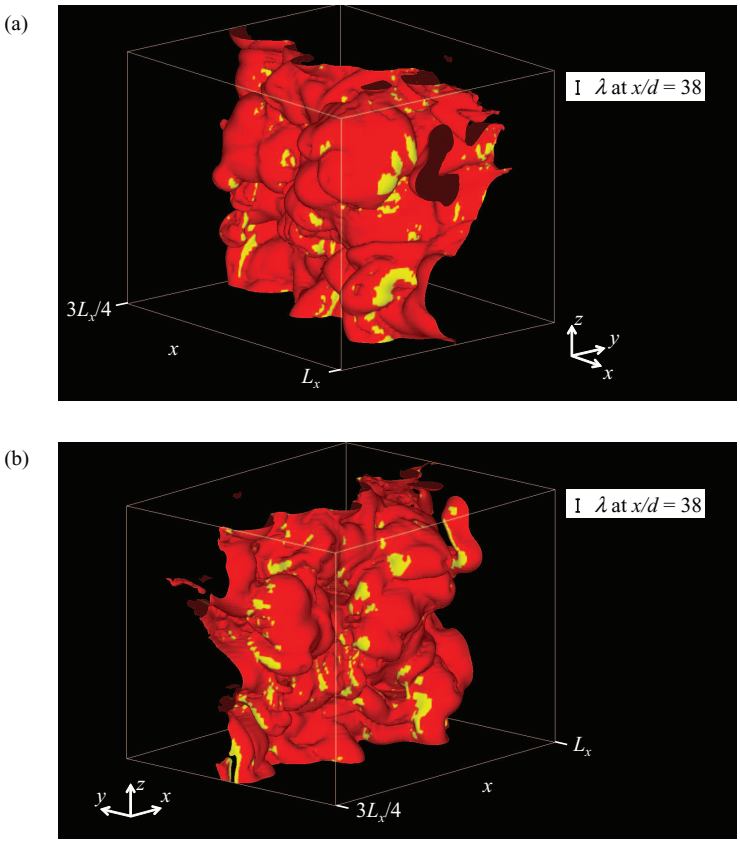

FIG. 15. Three-dimensional visualization of T/NT interface in the region $3L_x/4 \le x \le L_x$ and $y \le 0$. (a) View from downstream region. Yellow: leading edge. Red: other interface orientations. (b) View from upstream region. Yellow: trailing edge. Red: other interface orientations.

position of the jet flow in the turbulent region.[13] A sharp jump in $\langle|\boldsymbol{\omega}|b_U/U_C\rangle_I$ is observed near the T/NT interface, and $\langle|\boldsymbol{\omega}|b_U/U_C\rangle_I$ reaches a peak near the cross-streamwise edge at $y_I/\lambda = -0.7$ ($x/d = 20$) and $y_I/\lambda = -0.64$ ($x/d = 38$). The width of this vorticity jump is similar to that given by a DNS of a temporally developing planar jet.[13] $\langle|\boldsymbol{\omega}|b_U/U_C\rangle_I$ in the turbulent region hardly changes from $x/d = 20$ to 38. We see that there is a difference in the $\langle|\boldsymbol{\omega}|b_U/U_C\rangle_I$ values of the three interface

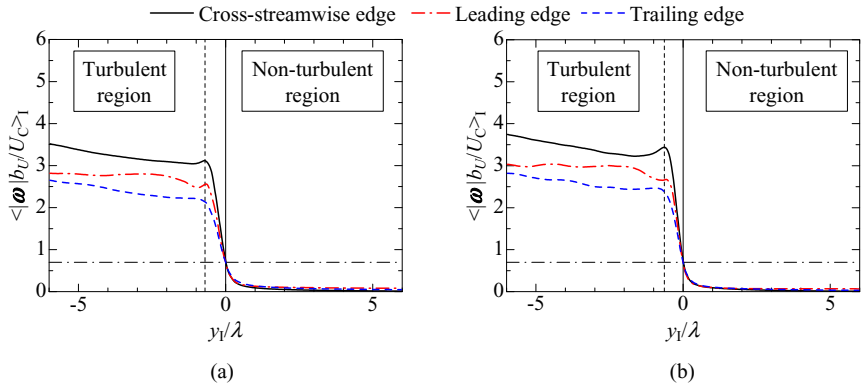

FIG. 16. Conditional mean normalized vorticity magnitude near T/NT interface detected at (a) $x/d = 20$ and (b) $x/d = 38$. The interface detection threshold $|\boldsymbol{\omega}|b_U/U_C = 0.7$ is shown by a horizontal dashed-dotted line. A vertical broken line shows the location of a peak of $\langle|\boldsymbol{\omega}|b_U/U_C\rangle_I$ near the cross-streamwise edge ($y_I/\lambda = -0.64$).

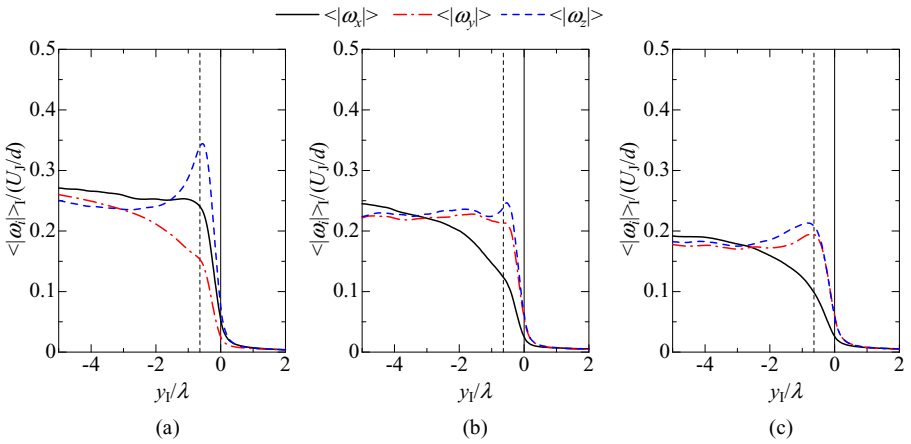

FIG. 17. Conditional average of magnitude of vorticity vector component ω_i near (a) cross-streamwise edge, (b) leading edge, and (c) trailing edge detected at $x/d = 38$. A vertical broken line shows $y_I/\lambda = -0.64$.

orientations in the turbulent region, but the widths of the vorticity jump are similar. Note also that $\langle|\boldsymbol{\omega}|b_U/U_C\rangle_I$ near the trailing edge slowly increases toward the turbulent region. The interfaces detected around $x/d = 38$ are used to analyze the characteristics of the T/NT interface.

Figure 17 shows $\langle|\omega_i|\rangle_I$ near the interface. The results show that $\langle|\omega_z|\rangle_I$ is the strongest component and that the weakest component depends on the interface orientation: $\langle|\omega_y|\rangle_I$ near the cross-streamwise edge and $\langle|\omega_x|\rangle_I$ near the leading and trailing edges. The weakest component corresponds to the vorticity normal to the T/NT interface. A similar dependence on the interface orientation was observed in wakes investigated by Bisset *et al.*[8] Figure 17 reveals that the component $\langle|\omega_i|\rangle_I$ normal to the T/NT interface gradually increases from the non-turbulent region toward the turbulent region, the component parallel to the T/NT interface shows a sharp jump near the interface, and $\langle|\omega_z|\rangle_I$ peaks just inside the turbulent region. Near the cross-streamwise edge, $\langle|\omega_z|\rangle_I$ decreases rapidly after peaking. Furthermore, we also see that the lowest jump in $\langle|\omega_i|\rangle_I$ is near the trailing edge.

Figure 18 shows $\langle U\rangle_I$ and $\langle V\rangle_I$; note that V is defined as negative in the direction toward the jet centerline. In the non-turbulent region, the negative $\langle V\rangle_I$ for all interface orientations is related to engulfment and induced flow toward the jet flow due to the large-scale motion.[39] We also see that $\langle V\rangle_I$ takes large negative values near the trailing edge. In the turbulent region, $\langle V\rangle_I$ is positive near the cross-streamwise and leading edges, but it is negative in both regions near the trailing edge. The positive $\langle V\rangle_I$ in the turbulent region is caused by jet expansion into the ambient flow. As shown in Fig. 18(a), $\langle U\rangle_I$ is almost constant in the non-turbulent region near the cross-streamwise

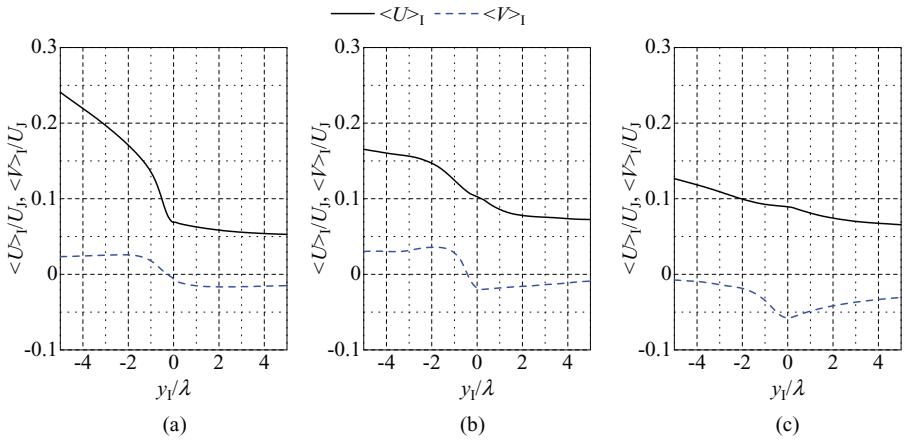

FIG. 18. Conditional average of streamwise velocity and lateral velocity near (a) cross-streamwise edge, (b) leading edge, and (c) trailing edge detected at $x/d = 38$.

edge, increases sharply from $y_I/\lambda = 0$ to -1, and then gradually increases toward the turbulent core region. The mean streamwise velocity of the ambient flow at $x = 0$ is $U_A = 0.056U_J$, which is nearly equal to $\langle U\rangle_I$ in the non-turbulent region near the cross-streamwise edge. However, near the leading and trailing edges, $\langle U\rangle_I$ is larger than U_A. The engulfing motion results in non-turbulent flows being caught between the leading and trailing edges, and another interface frequently appears on the non-turbulent side of these interfaces. As the turbulent flow has a faster streamwise velocity, in the non-turbulent region, $\langle U\rangle_I$ is larger than the free-stream value because the conditional statistics are calculated in the non-turbulent region close to the turbulent flow. Figure 18 also shows that the conditional average of the velocity normal to the interface (V for the cross-streamwise edge and U for the leading and trailing edges) in the turbulent region is larger than the velocity at the T/NT interface near the cross-streamwise and leading edges. In contrast, near the trailing edge, there is little difference in $\langle U\rangle_I$ in the two regions.

The conditional mean velocity in the non-turbulent region is significantly affected by large-scale motions such as engulfment and induced flow,[39] and large-scale motions in free shear flows will change depending on the flow configuration. For example, Philip and Marusic[39] pointed out that non-turbulent flow motions are dominated by different large-scale processes between jets and wakes and that induced flow due to large-scale motions is negligible in wakes.

C. Propagation velocity of the T/NT interface

Figure 19(a) shows $\langle v_n\rangle$ along with the contributions from enstrophy production $\langle v_P\rangle$, viscous effects $\langle v_{Vis}\rangle$, viscous diffusion $\langle v_D\rangle$, and viscous dissipation $\langle v_\epsilon\rangle$. The velocities are normalized by the Kolmogorov velocity $v_\eta = (\epsilon\nu)^{1/4}$ on the jet centerline. We found that $\langle v_n\rangle$ is small in comparison with v_η and that the smallest $\langle v_n\rangle$ is that at the trailing edge. Mean propagation of the T/NT interface into the non-turbulent region is observed at the cross-streamwise and leading edges (as indicated by the positive values), while there is on average no propagation into the non-turbulent region at the trailing edge. At the cross-streamwise and leading edges, we also see that $\langle v_{Vis}\rangle$ is small in comparison to $\langle v_P\rangle$. At the trailing edge, $\langle v_{Vis}\rangle$ contributes to the negative $\langle v_n\rangle$.

Recalling that $v_{Vis} = v_D + v_\epsilon$, we see that the T/NT interface propagates toward the turbulent region near the trailing edge because of viscous dissipation, i.e., the magnitude of $\langle v_D\rangle$ is smaller than that of $\langle v_\epsilon\rangle$. At both the cross-streamwise and leading edges, however, $\langle v_\epsilon\rangle$ and $\langle v_D\rangle$ are well balanced and so there is on average no propagation by viscous effects. The PDFs of v_n/v_η in Fig. 19(b) indicate that the leading edge tends to propagate toward the non-turbulent region faster than the other two interfaces. Although the PDF at the trailing edge does have positive v_n/v_η components, the propagation toward the turbulent region is faster.

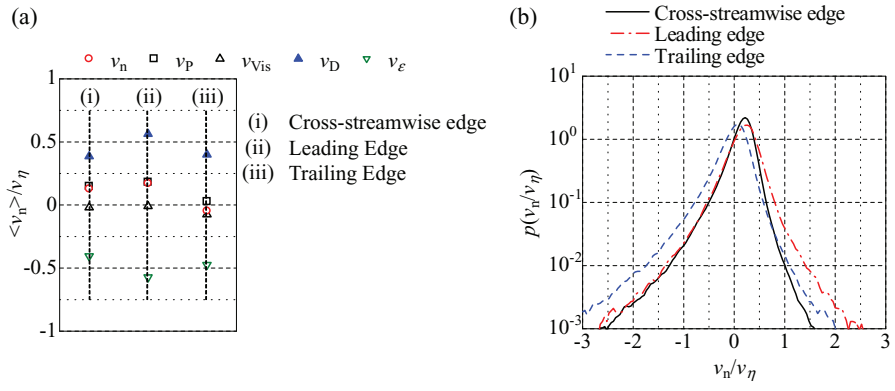

FIG. 19. Statistical properties of propagation velocity of T/NT interface at cross-streamwise edge, leading edge, and trailing edge detected at $x/d = 38$. (a) Mean propagation velocity normalized by Kolmogorov velocity v_η. Columns (i), (ii), and (iii) show mean propagation velocity at cross-streamwise edge, leading edge, and trailing edge, respectively. (b) Probability density function of propagation velocity.

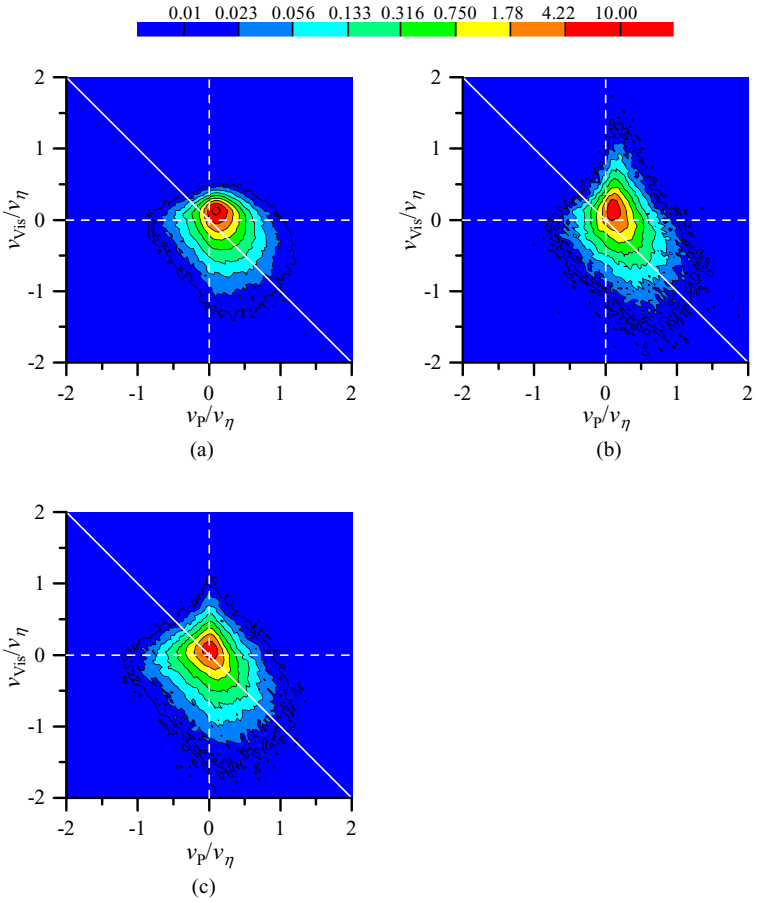

FIG. 20. Joint probability density functions of v_P and v_{Vis} at (a) cross-streamwise edge, (b) leading edge, and (c) trailing edge detected at $x/d = 38$. White solid lines: $v_n = v_P + v_{Vis} = 0$.

Figure 20 shows joint PDFs of v_P and v_{Vis} normalized by v_η. The white solid lines show $v_n = v_P + v_{Vis} = 0$, and the area above the line corresponds to positive v_n. For all interface orientations, the PDF peaks at a positive v_n value, but the peak for the trailing edge is closer to $v_n = 0$. These results are consistent with those in Fig. 19(b). For the positive v_{Vis}, the PDF is large for the positive v_n and the viscous effects cause the interface propagation to the non-turbulent region. Similarly, the positive v_P also contributes the positive v_n. We see that when v_{Vis} is negative, v_P tends to be positive, and thus enstrophy reduction by the viscous effects is often compensated for by enstrophy production by inviscid processes. However, at the trailing edge, v_P frequently becomes negative although the mean value is slightly positive as shown in Fig. 19(a). When v_P is negative, v_n tends to be negative especially at the trailing edge. Thus, enstrophy reduction by both inviscid and viscous processes contributes to a negative v_n and causes the interface to propagate toward the turbulent region.

The velocity relative to the movement of the T/NT interface appears in the transport equations in the form of $\mathbf{U} - \mathbf{U}^I$ and is important in the advection near the T/NT interface. Figure 21 shows the PDF of the relative velocity normal to the T/NT interface ($V - U_y^I$ for the cross-streamwise edge and $U - U_x^I$ for the leading and trailing edges) at $y_I/\lambda = -0.3$, -0.6, and -2.0. Note that a positive (negative) relative velocity in the turbulent region represents a velocity toward the T/NT interface near the cross-streamwise and leading (trailing) edges. The results show that while the relative velocity normal to the cross-streamwise and leading edges tends to be positive (toward the T/NT interface) it decreases in magnitude close to the interface. In contrast, the PDF of $U - U_x^I$ near the trailing edge is nearly symmetric about zero. The relative velocity of turbulent flow toward the cross-streamwise edge is related to jet expansion, and outward motion of turbulent flow was

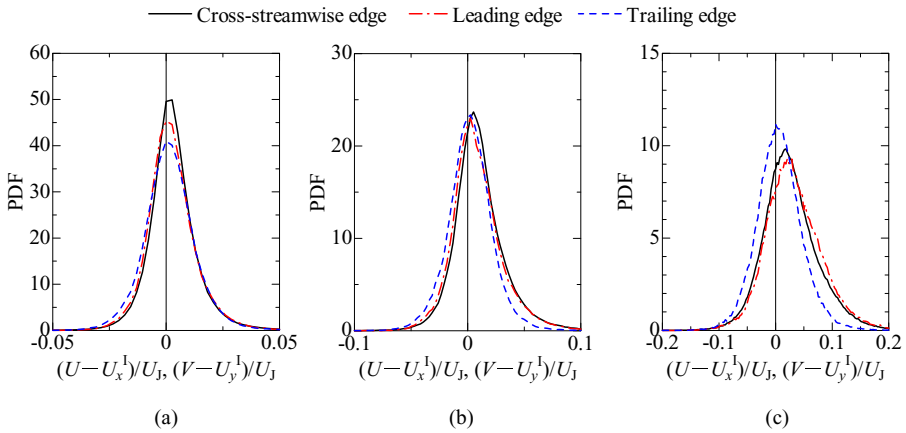

FIG. 21. Probability density function of relative velocity normal to T/NT interface detected at $x/d = 38$. (a) $y_{\mathrm{I}}/\lambda = -0.3$. (b) $y_{\mathrm{I}}/\lambda = -0.6$. (c) $y_{\mathrm{I}}/\lambda = -2.0$.

also observed in the conditional mean velocity in Fig. 18(a). Turbulent flow with a fast streamwise velocity is located up- and downstream of the leading and trailing edges, respectively, and tends to move toward the leading edge. Thus, the relative velocity will also depend on the location relative to these two interfaces.

Figure 22 shows the PDF of the relative velocity tangential to the T/NT interface, defined as $U - U_x^{\mathrm{I}}$ for the cross-streamwise edge and $V - U_y^{\mathrm{I}}$ for the leading and trailing edges. As was seen in Fig. 18(a), the streamwise velocity increases toward the turbulent core region near the cross-streamwise edge, and this is reflected in the PDF of $U - U_x^{\mathrm{I}}$ in that $U - U_x^{\mathrm{I}}$ is mainly positive. We also see that the streamwise velocity in the turbulent region is faster than the streamwise velocity of the T/NT interface. Note that the tangential movement of the T/NT interface is caused by the fluid velocity and not the propagation velocity. At the leading and trailing edges, Figs. 18(b) and 18(c) show that the conditional mean cross-streamwise velocity is negative at $y_{\mathrm{I}}/\lambda = 0$ and that the interface moves toward the inner region of the jet because of engulfing motion. The jet flow, however, expands into the ambient flow with jet development, and thus turbulent flow moves in a direction opposite to that of the interface movement. The PDFs show that the relative velocity $V - U_y^{\mathrm{I}}$ tends to be positive near the leading and trailing edges, and at $y_{\mathrm{I}}/\lambda = -0.6$, the relative velocity near the leading edge is larger than that near the trailing edge. However, at $y_{\mathrm{I}}/\lambda = -2.0$, there is little difference in the PDFs of $V - U_y^{\mathrm{I}}$ at the leading and trailing edges. A comparison of Figs. 21 and 22 reveals that turbulent flow near the interface tends on average

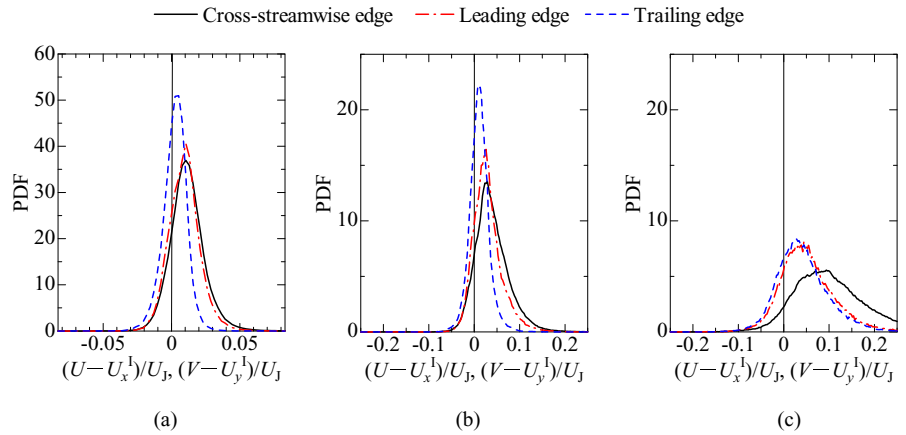

FIG. 22. Probability density function of relative velocity tangential to T/NT interface detected at $x/d = 38$. (a) $y_{\mathrm{I}}/\lambda = -0.3$. (b) $y_{\mathrm{I}}/\lambda = -0.6$. (c) $y_{\mathrm{I}}/\lambda = -2.0$.

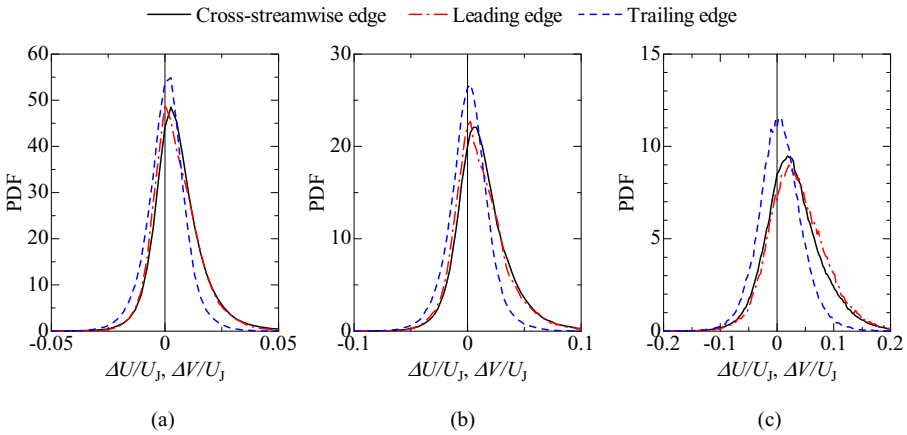

FIG. 23. Probability density function of difference in fluid velocity normal to T/NT interface between interface and turbulent region. The PDF is calculated from the T/NT interface detected at $x/d = 38$. (a) $y_I/\lambda = -0.3$. (b) $y_I/\lambda = -0.6$. (c) $y_I/\lambda = -2.0$.

to move in the tangential direction. A similar tendency was also observed by Taveira *et al.*[18] in the motion of fluid particles in a DNS of a temporally developing jet.

The instantaneous relative velocity normal to the interface can take large non-zero values even near the interface as shown in Fig. 21. The relative velocity is $\mathbf{U}(\mathbf{x}) - \mathbf{U}(\mathbf{x}_0^I) - \mathbf{V}^P$, and to determine whether the largest contribution is $\mathbf{V}^P$ or the fluid velocity difference $\Delta\mathbf{U} = \mathbf{U}(\mathbf{x}) - \mathbf{U}(\mathbf{x}_0^I)$, we calculate the PDF of $\Delta\mathbf{U}$ normal to the interface (Fig. 23). The PDF of the tangential component of $\Delta\mathbf{U}$ is the equal to that in Fig. 22 because $\mathbf{V}^P$ is normal to the T/NT interface. For the cross-streamwise edge, the fluid velocity difference in the interface normal direction is $\Delta V = V(\mathbf{x}) - V(\mathbf{x}_0^I)$, while it is $\Delta U = U(\mathbf{x}) - U(\mathbf{x}_0^I)$ for the leading and trailing edges. The PDFs of ΔU and ΔV are similar to the PDFs of the relative velocity shown in Fig. 21. Thus, the relative velocity near the interface is mainly caused by the fluid velocity difference. However, there are small differences between Figs. 21 and 23 at $y_I/\lambda = -0.3$. Interface propagation is important in the relative velocity in the region very close to the T/NT interface because the difference in the fluid velocity between the interface location and the turbulent region is small.

D. Enstrophy transport near the T/NT interface

The enstrophy transport mechanism near the T/NT interface is investigated by calculating the conditional average of the enstrophy transport equation, Eq. (28). Figure 24 shows the conditionally averaged terms of the enstrophy transport equation normalized by U_J and d. The conditional profile of the viscous diffusion term shows that viscous diffusion contributes to the conditional mean temporal variation in the enstrophy near the T/NT interface but is negligible away from the interface. On average, enstrophy production almost balances viscous dissipation in the turbulent region of $y_I/\lambda < -1$; this has also been observed by Taveira *et al.*[18] The temporal variation in the enstrophy is almost the same as the advection term in the turbulent region, and away from the interface, the same enstrophy transport characteristics are observed for the three interface orientations. In contrast, enstrophy transport near the T/NT interface depends strongly on the orientation of the interface: Near the cross-streamwise and leading edges, enstrophy production, which peaks at $y_I/\lambda \approx -0.5$, exceeds viscous dissipation, whereas near the trailing edge, enstrophy production is lower and decreases from the turbulent region toward the T/NT interface. Furthermore, the conditional profile of the advection term also depends strongly on the interface orientations; the advection term contributes to enstrophy growth near the cross-streamwise and leading edges, but near the trailing edge, it is negative in the region of $y_I/\lambda \approx -0.6$. This behavior of the advection term is related to the velocity relative to the T/NT interface (Figs. 21 and 22). In the turbulent region near the cross-streamwise and leading edges, the relative velocity transports enstrophy toward the T/NT interface, but near the

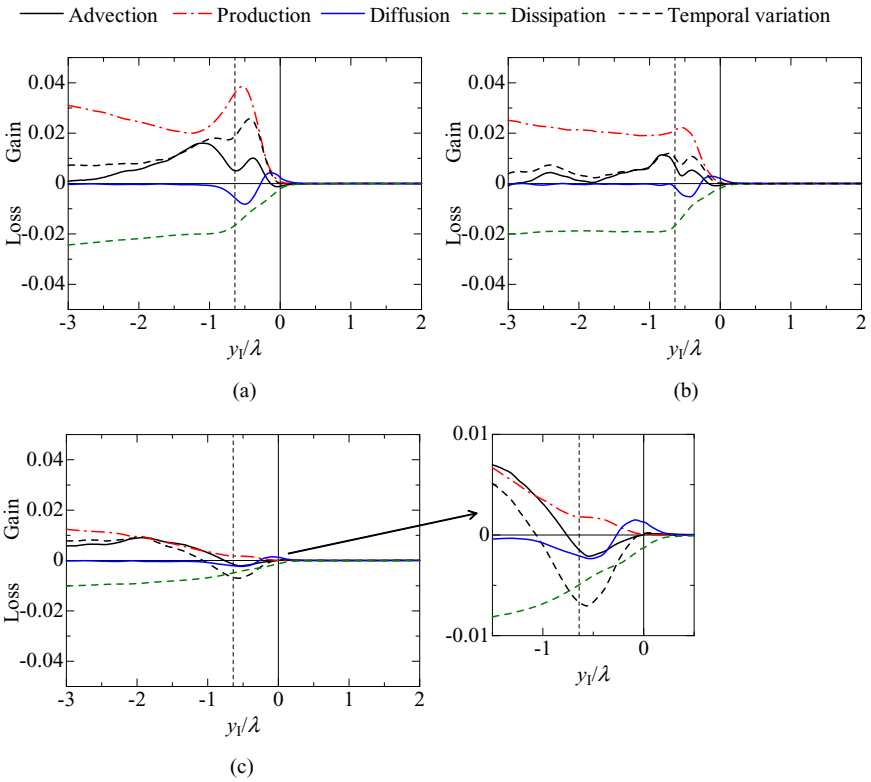

FIG. 24. Conditionally averaged terms of enstrophy transport equation near (a) cross-streamwise edge, (b) leading edge, and (c) trailing edge detected at $x/d = 38$. An enlargement of (c) is also shown for investigating the enstrophy transport. A vertical broken line shows $y_I/\lambda = -0.64$.

trailing edge, as the mean relative velocity toward the T/NT interface is nearly zero, the advection term does not on average contribute to enstrophy growth near the trailing edge.

The conditional average of the viscous diffusion term for all three interface orientations is positive in the region very close to the T/NT interface and negative just inside the turbulent region, and the viscous diffusion makes the largest contribution to enstrophy growth in the region very close to the T/NT interface, in agreement with previous results.[9,15,18] The dominance of the viscous effects in the enstrophy transport implies the existence of a laminar superlayer.[40] Near the cross-streamwise and leading edges, the conditional average of the viscous diffusion term is negative in the region in which enstrophy production and the advection term are positive. Thus, viscous diffusion transports, toward the non-turbulent region, enstrophy that is advected from the turbulent core region or produced just inside the T/NT interface. Note that a change in the Reynolds number may alter the enstrophy transport by viscous diffusion near the interface. However, because the DNS is performed for a planar jet with a relatively low Reynolds number, the role of viscous diffusion in enstrophy transport at high Reynolds numbers remains unclear and should be addressed in future works.

As a result of this enstrophy transport, the conditional average of the temporal variation is positive near the cross-streamwise and leading edges and negative near the trailing edge. The tendency for the enstrophy to decrease in the turbulent region near the trailing edge is consistent with the small conditional mean vorticity magnitude, as shown in Fig. 16. Because the T/NT interface can be represented by an enstrophy isosurface, interface propagation occurs owing to enstrophy growth in the non-turbulent region or enstrophy reduction in the turbulent region. The conditional average of the enstrophy transport equation shows that enstrophy growth by viscous diffusion near the cross-streamwise and leading edges causes the interface to propagate toward the non-turbulent region. The negative temporal variation in the turbulent region near the trailing edge is related to the interface propagation toward the turbulent region.

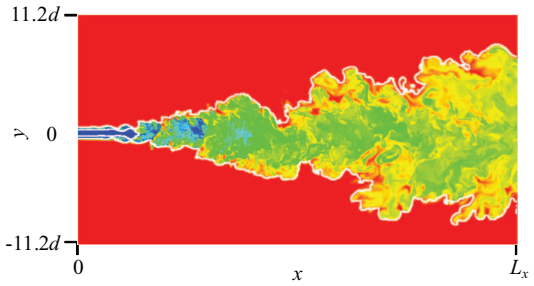

FIG. 25. Visualization of T/NT interface and scalar field. White lines represent T/NT interface. Color contour represents values of the scalar ϕ. Blue: $\phi = 0$. Red: $\phi = 1$.

E. Scalar transport near the T/NT interface

Figure 25 shows the instantaneous scalar field and T/NT interface. We see that the interface envelops the jet flow ($\phi < 1$) and defines the boundary between jet flow and ambient flow ($\phi \approx 1$). The value of ϕ in the jet flow increases in the downstream direction because the ambient flow is entrained into the jet flow with jet development. Figures 26(a) and 26(b) show $\langle\phi\rangle_I$ near the T/NT interface detected at $x/d = 20$ and 38, respectively. A sharp jump in $\langle\phi\rangle_I$ near the interface is observed for all three interface orientations, and the width of the jump is almost the same as that of the vorticity jump (Fig. 16). In the turbulent region, the largest value and smallest gradient of $\langle\phi\rangle_I$ is near the trailing edge, which is consistent with the instantaneous scalar field shown in Fig. 25.

The scalar transport mechanism near the T/NT interface is investigated using Eq. (30), and Fig. 27 shows the conditionally averaged terms of the scalar transport equation normalized by U_J and d. The conditional average of the molecular diffusion term is positive just inside the turbulent region, and is negative near the T/NT interface, indicating that the scalar near the T/NT interface is transported into the turbulent region by molecular diffusion. We also see that the conditional profile of the molecular diffusion term is almost independent of the interface orientation. Note that changes in the Schmidt and Reynolds numbers will have a significant effect on the molecular diffusion near the interface.

Even though the propagation velocity is not large, interface propagation plays an important role in scalar transport across the interface because of the large gradient of the scalar near the interface. At the cross-streamwise and leading edges, because the mean propagation velocity is positive (Fig. 19) and hence the T/NT interface propagates toward the non-turbulent region ($\phi \approx 1$), the conditional average of the advection term ($\nabla \cdot (\phi \mathbf{V}^P)$) at the interface is positive. Thus, ϕ in the non-turbulent region is transported across the T/NT interface into the turbulent region. Near the trailing edge, however, the turbulent flow often becomes non-turbulent because of enstrophy reduction (Fig. 24(c)).

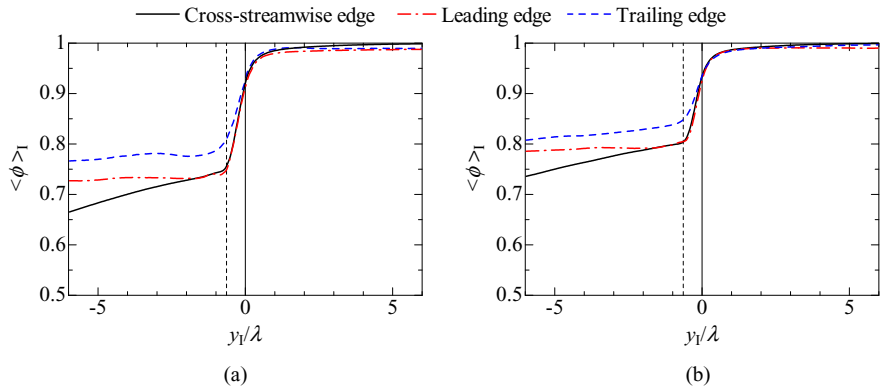

FIG. 26. Conditional average of ϕ near cross-streamwise edge, leading edge, and trailing edge detected at (a) $x/d = 20$ and (b) $x/d = 38$. The location of $y_I/\lambda = -0.64$ is shown by a vertical broken line.

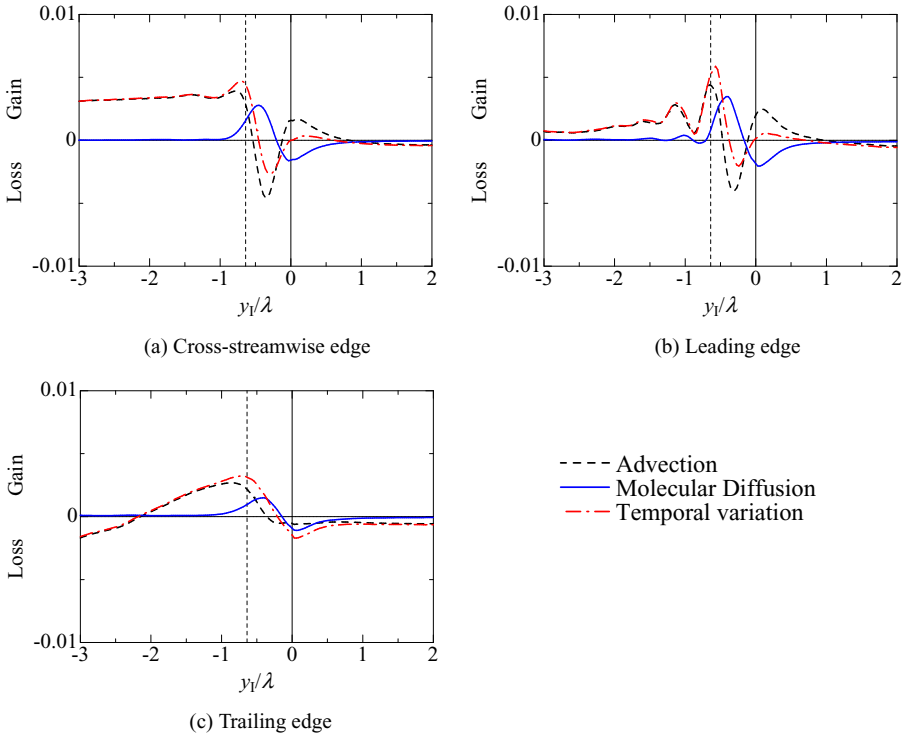

FIG. 27. Conditionally averaged terms of scalar transport equation near (a) cross-streamwise edge, (b) leading edge, and (c) trailing edge detected at $x/d = 38$.

As a result, the entrained scalar remains in the non-turbulent region, and the scalar in the turbulent region is transported across the interface. This results in a negative advection term at the interface. Fluids with a smaller scalar remain in the non-turbulent region when the interface propagates toward the turbulent region, and this promotes scalar mixing in the non-turbulent region as the scalar in the turbulent region is lower. These results show that the motion of the T/NT interface differs from that of the scalar interface (or scalar isosurface). The scalar flux across the T/NT interface is represented by $\phi\mathbf{V}^{\mathrm{P}}$, and the mean scalar fluxes at the cross-streamwise, leading, and trailing edges detected at $x/d = 38$ are $2.4 \times 10^{-3} U_{\mathrm{J}}$, $3.2 \times 10^{-3} U_{\mathrm{J}}$, and $-0.81 \times 10^{-3} U_{\mathrm{J}}$, respectively. These results confirm that ϕ is entrained into the turbulent region by interface propagation across the cross-streamwise and leading edges but not the trailing edge. Figure 27 indicates that both interface propagation and molecular diffusion contribute to the scalar transport across the T/NT interface.

As was shown in Fig. 21, the relative velocity toward the T/NT interface can be frequently observed in the turbulent region near the cross-streamwise and leading edges, and fluid with a small ϕ in the turbulent region is transported toward the interface. Therefore, the conditional average of the advection term is negative inside the turbulent region ($y_{\mathrm{I}}/\lambda \approx -0.5$ to -0.1) near the cross-streamwise and leading edges.

Figure 28 shows the joint PDFs of the advection and molecular diffusion terms of the scalar transport equation at the interface. At the cross-streamwise and leading edges, the advection and molecular diffusion terms are negatively correlated, and a large probability is associated with a positive advection term and a negative molecular diffusion term. These joint PDFs confirm that as the scalar is transported across the T/NT interface by interface propagation, molecular diffusion simultaneously transports the scalar into the turbulent region. Figure 28(c) shows that negative values of the advection term are frequently observed at the trailing edge, which is consistent with the entrained scalar remaining in the non-turbulent region when the interface propagates toward the turbulent region.

The spatial correlation of ϕ is analyzed to investigate the characteristics of ϕ near the T/NT interface. The cross-correlation function $C_{\phi\phi}(\delta, y_{\mathrm{I}})$ is calculated using the two points y_{I} and $y_{\mathrm{I}} + \delta$

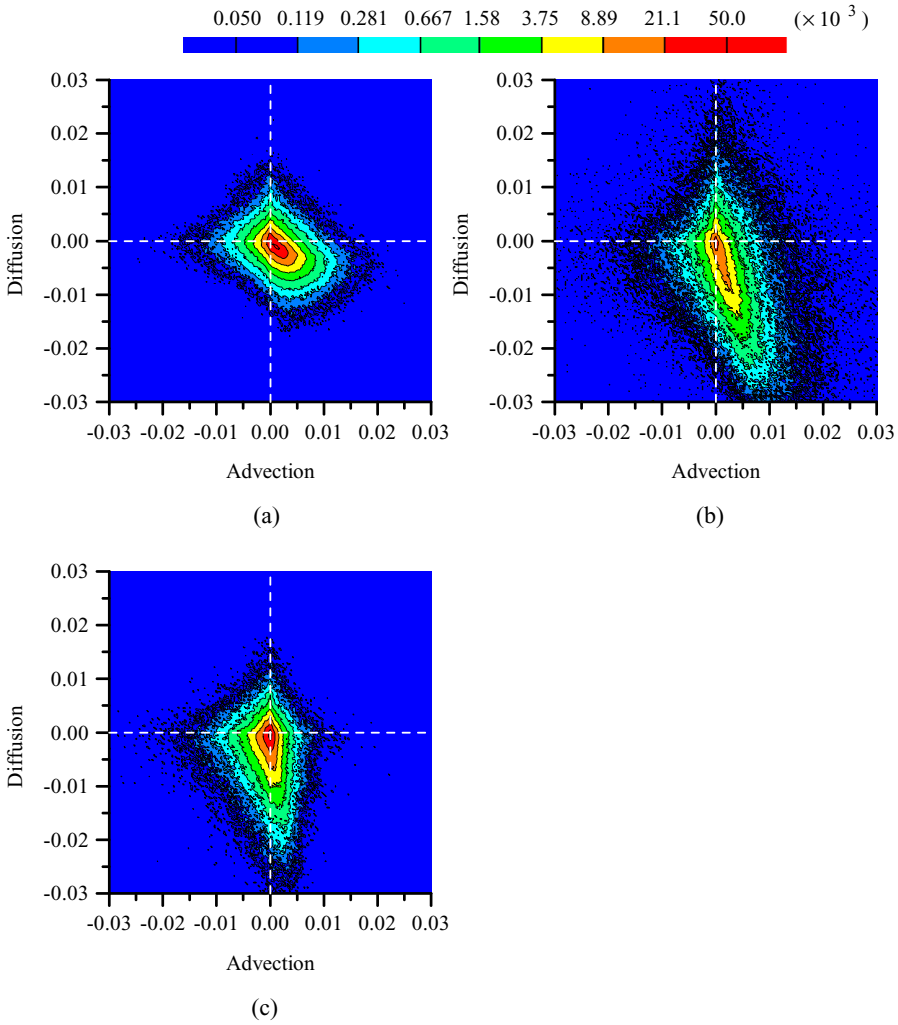

FIG. 28. Joint PDFs of advection and molecular diffusion terms in scalar transport equation at (a) cross-streamwise, (b) leading, and (c) trailing edges. These terms are normalized by U_J and d.

shown in Fig. 29,

$$C_{\phi\phi}(\delta, y_I) = \frac{\langle \phi'(y_I)\phi'(y_I+\delta)\rangle_I}{\langle \phi'^2(y_I)\rangle_I^{1/2}\langle \phi'^2(y_I+\delta)\rangle_I^{1/2}}, \tag{34}$$

where $\phi'(y_I) = \phi(y_I) - \langle\phi(y_I)\rangle_I$ is the fluctuation from the conditional average, and the cross-correlation is calculated using the same procedure as that for the conditional average. Figures 30(a)

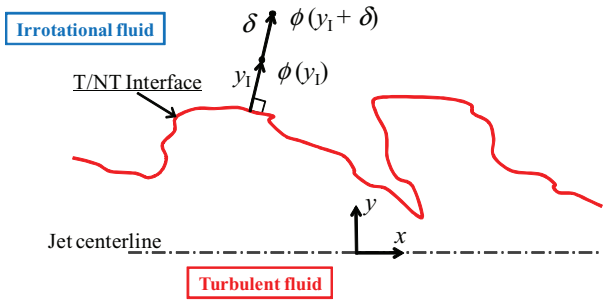

FIG. 29. Definition of two points used to define the cross-correlation function.

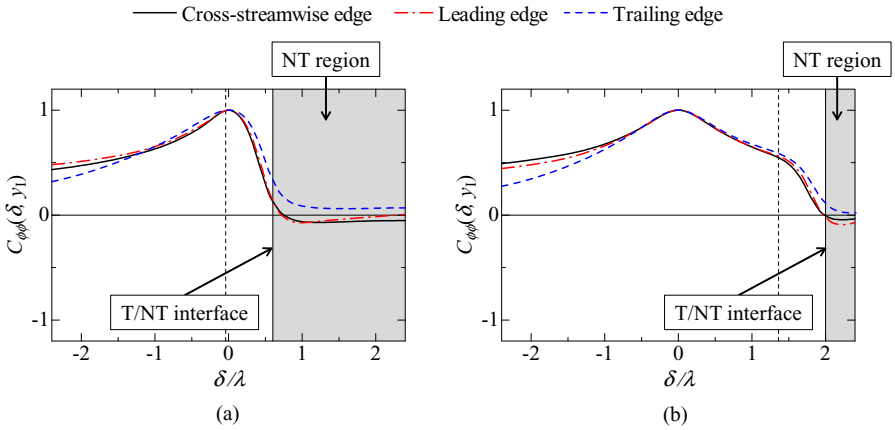

FIG. 30. Cross-correlation function $C_{\phi\phi}(\delta, y_I)$ at (a) $y_I/\lambda = -0.6$ and (b) $y_I/\lambda = -2.0$. Distance δ for which $y_I + \delta$ is in non-turbulent region is highlighted in gray. The location where vorticity magnitude near cross-streamwise edge reaches a peak value ($y_I/\lambda = -0.64$) is shown by a vertical broken line.

and 30(b) show $C_{\phi\phi}(\delta, y_I)$ at $y_I/\lambda = -0.6$ and -2.0, respectively. Note that the conditional mean vorticity magnitude near the cross-streamwise edge peaks near $y_I/\lambda = -0.6$ [Fig. 16(b)] and that $y_I/\lambda = -2.0$ is well inside the turbulent region. In the turbulent region, $C_{\phi\phi}(\delta, y_I)$ decreases gradually from $C_{\phi\phi}(0, y_I) = 1$ as $|\delta|$ increases but decreases rapidly in the region in which there is a sharp jump in the vorticity magnitude. There is little correlation between the scalar fluctuations of the turbulent region and the non-turbulent region away from the interface. The rapid decrease in $C_{\phi\phi}(\delta, y_I)$ near the interface is related to interface propagation, which means that fluid near the T/NT interface consists mainly of fluid arriving from the non-turbulent region. Molecular diffusion can result in scalar correlations between the turbulent region and the region near the T/NT interface. Although $C_{\phi\phi}$ decreases rapidly close to the interface, $C_{\phi\phi}$ is still positive near the interface, indicating that molecular diffusion affects the scalar transport near the interface. For a distance δ in the region in which a sharp jump in $|\boldsymbol{\omega}|$ is observed, the largest $C_{\phi\phi}(\delta, y_I)$ is that near the trailing edge. The trailing edge often propagates toward the turbulent region. When the T/NT interface propagates toward the turbulent region, the entrained scalar is left in the non-turbulent region. Thus, fluid from the turbulent region exists near the trailing edge, resulting in the large spatial correlation between the turbulent region and the region near the T/NT interface. The conditional average of the scalar transport equation and the sharp drop in $C_{\phi\phi}(\delta, y_I)$ near the T/NT interface indicate that ϕ is transported across the interface by interface propagation and that molecular diffusion also contributes to the transport near the interface.

V. CONCLUDING REMARKS

DNS of a planar jet was performed to investigate the enstrophy and passive scalar transports near the T/NT interface. We considered the transport of the passive scalar ϕ whose values in the jet exit and ambient flow are 0 and 1, respectively. The effect of the interface orientation on the characteristics of the T/NT interface was also investigated in detail. The main results of this paper are summarized as follows.

1. The cross-streamwise and leading edges frequently propagate toward the non-turbulent region because of the enstrophy production and the enstrophy growth caused by viscous diffusion. In contrast, the trailing edge frequently propagates toward the turbulent region because the enstrophy is significantly decreased by the viscous dissipation, which exceeds the enstrophy growth by the production and viscous diffusion near the trailing edge. Negative values of the enstrophy production also largely contribute to the interface propagation toward the turbulent region especially at the trailing edge.

2. The velocity relative to the interface movement in the turbulent region is frequently toward the T/NT interface near the cross-streamwise and leading edges. However, the mean relative velocity normal to the trailing edge in the turbulent region is nearly zero. The relative velocity of turbulent flows toward the cross-streamwise edge is related to the jet expansion. The difference between the leading and trailing edges is caused by the turbulent flows with fast streamwise velocity, which are located up- and downstream of the leading and trailing edges, respectively. The instantaneous relative velocity normal to the interface can be large, and this large relative velocity is caused by the difference in the fluid velocity between the interface location and the turbulent region rather than the interface propagation.
3. The conditional profiles of the enstrophy transport equation show the similar tendency to the previous studies by Holzner *et al.*[15] and Taveira *et al.*,[18] but in the present DNS, large differences were observed between the trailing edge and the cross-streamwise and leading edges. The conditional average of the enstrophy production peaks slightly inside the turbulent region near the cross-streamwise and leading edges. Near these interfaces, the advection term contributes to the enstrophy growth because the velocity field transports the enstrophy existing in the turbulent core region toward the T/NT interface. Viscous diffusion transports, toward the non-turbulent region, the enstrophy, that is advected from the turbulent core region or is produced slightly inside the T/NT interface. Near the trailing edge, the enstrophy production is small, and the conditional average of the temporal variation is negative. The enstrophy reduction near the trailing edge results in interface propagation of the trailing edge toward the turbulent region.
4. Both the interface propagation and the molecular diffusion contribute to the scalar transport across the T/NT interface. The passive scalar ϕ in the non-turbulent region is frequently transported into the turbulent region across the cross-streamwise and leading edges by interface propagation toward the non-turbulent region. Contrary to these two interface orientations, ϕ in the turbulent region is transported into the non-turbulent region across the trailing edge. When the T/NT interface propagates toward the turbulent region, the entrained scalar remains in the non-turbulent region. The spatial correlation of ϕ near the T/NT interface indicates that fluid near the interface consists mainly of fluid arriving from the non-turbulent region.

ACKNOWLEDGMENTS

The authors acknowledge Professor C. B. da Silva and Mr. R. R. Taveira for providing valuable comments. The authors also acknowledge the anonymous referees for valuable comments. The authors would like to thank Dr. O. Terashima for his help in this study. Part of this work was conducted under the Collaborative Research Project of the Institute of Fluid Science, Tohoku University. This work was supported by JSPS KAKENHI Grant No. 25002531 and MEXT KAKENHI Grant Nos. 25289030, 25289031, and 25630052.

[1] C. B. da Silva, J. C. R. Hunt, I. Eames, and J. Westerweel, "Interfacial layers between regions of different turbulence intensity," Annu. Rev. Fluid Mech. **46**, 567 (2014).
[2] R. W. Bilger, "Turbulent jet diffusion flames," Prog. Energy Combust. Sci. **1**, 87 (1976).
[3] R. W. Bilger, "Turbulent diffusion flames," Annu. Rev. Fluid Mech. **21**, 101 (1989).
[4] J. Westerweel, T. Hofmann, C. Fukushima, and J. C. R. Hunt, "The turbulent/non-turbulent interface at the outer boundary of a self-similar turbulent jet," Exp. Fluids **33**, 873 (2002).
[5] J. Westerweel, C. Fukushima, J. M. Pedersen, and J. C. R. Hunt, "Mechanics of the turbulent-nonturbulent interface of a jet," Phys. Rev. Lett. **95**, 174501 (2005).
[6] J. Westerweel, C. Fukushima, J. M. Pedersen, and J. C. R. Hunt, "Momentum and scalar transport at the turbulent/non-turbulent interface of a jet," J. Fluid Mech. **631**, 199 (2009).
[7] M. Gampert, K. Kleinheinz, N. Peters, and H. Pitsch, "Experimental and numerical study of the scalar turbulent/non-turbulent interface layer in a jet flow," Flow, Turbul. Combust. **92**, 429 (2014).
[8] D. K. Bisset, J. C. R. Hunt, and M. M. Rogers, "The turbulent/non-turbulent interface bounding a far wake," J. Fluid Mech. **451**, 383 (2002).
[9] C. B. da Silva and J. C. F. Pereira, "Invariants of the velocity-gradient, rate-of-strain, and rate-of-rotation tensors across the turbulent/nonturbulent interface in jets," Phys. Fluids **20**, 055101 (2008).
[10] C. B. da Silva and J. C. F. Pereira, "The effect of subgrid-scale models on the vortices computed from large-eddy simulations," Phys. Fluids **16**, 4506 (2004).

[11] C. B. da Silva and R. R. Taveira, "The thickness of the turbulent/nonturbulent interface is equal to the radius of the large vorticity structures near the edge of the shear layer," Phys. Fluids **22**, 121702 (2010).
[12] C. B. da Silva, R. J. N. Dos Reis, and J. C. F. Pereira, "The intense vorticity structures near the turbulent/non-turbulent interface in a jet," J. Fluid Mech. **685**, 165 (2011).
[13] R. R. Taveira and C. B. da Silva, "Kinetic energy budgets near the turbulent/nonturbulent interface in jets," Phys. Fluids **25**, 015114 (2013).
[14] J. Mathew and A. J. Basu, "Some characteristics of entrainment at a cylindrical turbulence boundary," Phys. Fluids **14**, 2065 (2002).
[15] M. Holzner, A. Liberzon, N. Nikitin, B. Lüthi, W. Kinzelbach, and A. Tsinober, "A Lagrangian investigation of the small-scale features of turbulent entrainment through particle tracking and direct numerical simulation," J. Fluid Mech. **598**, 465 (2008).
[16] M. Holzner, B. Lüthi, A. Tsinober, and W. Kinzelbach, "Acceleration, pressure and related quantities in the proximity of the turbulent/non-turbulent interface," J. Fluid Mech. **639**, 153 (2009).
[17] M. Holzner and B. Lüthi, "Laminar superlayer at the turbulence boundary," Phys. Rev. Lett. **106**, 134503 (2011).
[18] R. R. Taveira, J. S. Diogo, D. C. Lopes, and C. B. da Silva, "Lagrangian statistics across the turbulent-nonturbulent interface in a turbulent plane jet," Phys. Rev. E **88**, 043001 (2013).
[19] M. A. C. Teixeira and C. B. da Silva, "Turbulence dynamics near a turbulent/non-turbulent interface," J. Fluid Mech. **695**, 257 (2012).
[20] T. Watanabe, Y. Sakai, K. Nagata, O. Terashima, H. Suzuki, T. Hayase, and Y. Ito, "Visualization of turbulent reactive jet by using direct numerical simulation," Int. J. Model. Simul. Sci. Comput. **4**, 1341001 (2013).
[21] J. C. R. Hunt, I. Eames, and J. Westerweel, "Mechanics of inhomogeneous turbulence and interfacial layers," J. Fluid Mech. **554**, 499 (2006).
[22] Y. Morinishi, T. S. Lund, O. V. Vasilyev, and P. Moin, "Fully conservative higher order finite difference schemes for incompressible flow," J. Comput. Phys. **143**, 90 (1998).
[23] P. R. Spalart, R. D. Moser, and M. M. Rogers, "Spectral methods for the Navier-Stokes equations with one infinite and two periodic directions," J. Comput. Phys. **96**, 297 (1991).
[24] Y. Dai, T. Kobayashi, and N. Taniguchi, "Large eddy simulation of plane turbulent jet flow using a new outflow velocity boundary condition," JSME Int. J. Ser. B **37**, 242 (1994).
[25] T. Watanabe, Y. Sakai, K. Nagata, O. Terashima, and T. Kubo, "Simultaneous measurements of reactive scalar and velocity in a planar liquid jet with a second-order chemical reaction," Exp. Fluids **53**, 1369 (2012).
[26] T. Watanabe, Y. Sakai, K. Nagata, and O. Terashima, "Joint statistics between velocity and reactive scalar in a turbulent liquid jet with a chemical reaction," Phys. Scr. **T155**, 014039 (2013).
[27] T. Watanabe, Y. Sakai, K. Nagata, and O. Terashima, "Turbulent Schmidt number and eddy diffusivity change with a chemical reaction," J. Fluid Mech. **754**, 98 (2014).
[28] T. Watanabe, Y. Sakai, K. Nagata, and O. Terashima, "Experimental study on the reaction rate of a second-order chemical reaction in a planar liquid jet," AIChE J. **60**, 3969 (2014).
[29] H. Abe, Y. Matsuo, and H. Kawamura, "Direct numerical simulation of a fully developed turbulent channel flow with respect to the Reynolds number dependence," J. Fluids Eng. **123**, 382 (2001).
[30] S. B. Pope, *Turbulent Flows* (Cambridge University Press, Cambridge, 2000).
[31] M. Klein, A. Sadiki, and J. Janicka, "A digital filter based generation of inflow data for spatially developing direct numerical or large eddy simulations," J. Comput. Phys. **186**, 652 (2003).
[32] A. Kempf, M. Klein, and J. Janicka, "Efficient generation of initial-and inflow-conditions for transient turbulent flows in arbitrary geometries," Flow, Turbul. Combust. **74**, 67 (2005).
[33] E. Gutmark and I. Wygnansk, "The planar turbulent jet," J. Fluid Mech. **73**, 465 (1976).
[34] B. R. Ramaprian and M. S. Chandrasekhara, "LDA measurements in plane turbulent jets," J. Fluids Eng. **107**, 264 (1985).
[35] S. A. Stanley, S. Sarkar, and J. P. Mellado, "A study of the flow-field evolution and mixing in a planar turbulent jet using direct numerical simulation," J. Fluid Mech. **450**, 377 (2002).
[36] M. Klein, A. Sadiki, and J. Janicka, "Investigation of the influence of the Reynolds number on a plane jet using direct numerical simulation," Int. J. Heat Fluid Flow **24**, 785 (2003).
[37] A. E. Davies, J. F. Keffer, and W. D. Baines, "Spread of a heated plane turbulent jet," Phys. Fluids **18**, 770 (1975).
[38] T. Watanabe, Y. Sakai, K. Nagata, Y. Ito, and T. Hayase, "Wavelet analysis of coherent vorticity near the turbulent/non-turbulent interface in a turbulent planar jet," Phys. Fluids **26**, 095105 (2014).
[39] J. Philip and I. Marusic, "Large-scale eddies and their role in entrainment in turbulent jets and wakes," Phys. Fluids **24**, 055108 (2012).
[40] S. Corrsin and A. L. Kistler, "Free-stream boundaries of turbulent flows," NACA Technical Report No. TN-1244, 1955.